

Amin Alirezaylavasani

**Genetic interaction between accessory non-homologous end joining factors in B and T lymphocyte development**

Master's thesis in Molecular Medicine

Supervisor: Dr. Valentyn Oksenysh

Co-supervisor: Sergio Castañeda-Zegarra

April 2020

**NTNU**  
Norwegian University of Science and Technology  
Faculty of Medicine and Health Sciences  
Department of Clinical and Molecular Medicine



Norwegian University of  
Science and Technology

## Table of contents

<b>Abstract</b>	<b>4</b>
<b>Acknowledgment</b>	<b>5</b>
<b>Abbreviations</b>	<b>6</b>
<b>Preface</b>	<b>8</b>
<b>1. Introduction</b>	<b>9</b>
1.1 V(D)J recombination	13
1.2 Class switch recombination	19
1.3 B and T cell development associated diseases in humans	22
<b>2. Hypotheses and research aims</b>	<b>24</b>
<b>3. Material and Methods</b>	<b>25</b>
3.1 Mouse models	25
3.2 Genotyping	25
3.2.1 DNA extraction and Polymerase Chain Reaction (PCR)	25
3.2.2 Electrophoresis	25
3.3. Count of cells isolated from the lymphoid organs	26
3.4. Cell staining for Flow Cytometry analysis	27
3.5 Statistics	28
<b>4. Results</b>	<b>29</b>
4.1 Genotyping	29
4.2 Immune system development in <i>Xlf<sup>-/-</sup>Paxx<sup>-/-</sup>Trp53<sup>+/-</sup></i> mice	32
4.3 B and T cell development in <i>Xlf<sup>-/-</sup>Paxx<sup>-/-</sup>Trp53<sup>+/-</sup></i> mice	36
4.4 Genetic interaction between <i>Mri</i> and <i>Dna-pkcs</i> genes in mice	44
4.5 No genetic interaction between <i>Mri</i> and <i>Paxx</i> genes in mice	46
4.6 Proportions of B and T lymphocytes in spleens, thymi and bone marrow of <i>Mri<sup>-/-</sup>Paxx<sup>-/-</sup></i> mice	50
<b>5. Discussion</b>	<b>57</b>
5.1 <i>Xlf<sup>-/-</sup>Paxx<sup>-/-</sup>Trp53<sup>+/-</sup></i> deficiency leads to deficient B and T cell development	57
5.2 <i>Mri<sup>-/-</sup>Dna-pkcs<sup>-/-</sup></i> double deficiency leads to embryonic lethality	58
5.3 There is no genetic interaction between <i>Mri</i> and <i>Paxx</i> genes in mice	59
<b>6. Conclusion</b>	<b>60</b>
<b>7. Future directions</b>	<b>61</b>
<b>8. References</b>	<b>62</b>
<b>9. Supplementary information</b>	<b>65</b>
9.1 Appendix A	65

<b>9.2 Appendix B</b>	<b>66</b>
<b>9.3 Appendix C</b>	<b>66</b>

## Abstract

DNA double-strand breaks (DSBs) are induced by exogenous and endogenous factors. Non-homologous end-joining (NHEJ) pathway is a repair system that deals with DSBs all over the cell cycle. NHEJ is required for V(D)J recombination in developing B and T cells, and for class switch recombination (CSR) in mature B lymphocyte. NHEJ core factors Ku70/80 form a heterodimer complex that associates with DSB and facilitates the recruitment of downstream core factors such as X-ray repair cross-complementing group 4 (XRCC4), XRCC4-like factor (XLF) and DNA ligase 4 (Lig4). Assembly of Ku heterodimer also recruits the accessory factors (e.g., PAXX, Mri/Cyren and DNA-PKcs) as well.

Deficiency of core NHEJ elements results in lack of mature B and T cells in spleen and thymus due to V(D)J recombination failure. On the other hand, mutation in the genes encoding for the accessory factors like *Paxx* and *Mri*, leads to normal phenotype or only have a minor effect. Combined inactivation of *Xlf* and *Paxx* genes results in late embryonic lethality in mice. Inactivation of one or both alleles of *Trp53* rescues the embryonic lethality of *Xlf<sup>-/-</sup>Paxx<sup>-/-</sup>* mice and allows postnatal survival. *Xlf<sup>-/-</sup>Paxx<sup>-/-</sup>Trp53<sup>+/-</sup>* mice possess no mature B cells and very few mature T cells in the lymphoid organs.

V(D)J recombination insufficiency results in accumulation of pro-B cells in the bone marrow of mice lacking XLF, PAXX and p53 proteins. Observed data allowed me to conclude that deficient B cell development in *Xlf<sup>-/-</sup>Paxx<sup>-/-</sup>Trp53<sup>+/-</sup>* mice, originates from the bone marrow. Following, genetic interaction study revealed that *Mri* and *Dna-pkcs* have overlapping functions. Contrary, there is no genetic interaction between *Mri* and *Paxx* genes in mice.

## **Acknowledgment**

I want to thank my supervisor Dr. Valentyn Oksenykh for his support and for giving me the opportunity to join his group. He cares about his students and our success is his success. I developed my skills because of his guidance and I deeply appreciate that he constantly encouraged me and takes the time to give through supervision and close follow up.

Special thanks to my co-supervisor Sergio Miguel Castaneda Zegarra, PhD candidate in the Oksenykh research group, due to his numerous theoretical and practical guidances that lead me to accomplish my thesis precisely.

I would like to thank Qindong Zhang and Kalaiyarasi Rangunathan, my colleagues in the Oksenykh research group for their help and collaboration during my study.

If we consider the aim of the master study, learning how to perform research, improving the theoretical and practical knowledge, the practice of soft skills, or generally, become ready for the future steps in academic and social life; I learned, practiced and experienced them in Oksenykh research group and I am extremely thankful for that.

## Abbreviations

- **A-EJ** Alternative end-joining
- **AID** Activation-induced cytidine deaminase
- **CNS** Central nervous system
- **CSR** Class switch recombination
- **DDR** DNA damage response
- **ddH<sub>2</sub>O** Double Distilled Water
- **DNA** Deoxyribonucleic acid
- **DNA-PKcs** DNA-dependent protein kinase catalytic subunit
- **DSBs** Double-strand breaks (of DNA)
- **G<sub>1</sub> phase** Gap 1 phase of the cell cycle
- **G<sub>2</sub> phase** Gap 2 phase of the cell cycle
- **GI** Genetic interaction
- **H2AX** H2A histone family member X
- **HR** Homologous recombination
- **IgH** Immunoglobulin heavy chain
- **IgL** Immunoglobulin light chain
- **Ku70/80** Ku70/80 heterodimer
- **Lig4** DNA ligase 4
- **Mri** Modulator of retrovirus infection homolog 1
- **MRN** MRE11-RAD50-NBS1
- **Mut** Mutagenic
- **NHEJ** Non-homologous end-joining
- **nt** Nucleotide
- **OS** Omenn syndrome
- **PARP1** Poly (ADP-ribose) polymerase 1
- **PAXX** Paralog of XRCC4 and XLF
- **Pol** Polymerase
- **PCR** Polymerase chain reaction
- **RAD50** DNA repair protein RAD50
- **S** Switch region
- **S phase** Synthesis phase

- **SCID** Severe combined immunodeficiency
- **SSBs** Single-strand breaks
- **ssDNA** Single-stranded DNA
- **TF** Transcription factor
- ***Trp53*** Tumor protein 53 gene
- **UV** Ultraviolet
- **WS** Werner syndrome
- **WT** Wild-type
- **XLF** XRCC4-like factor
- **XRCC4** X-ray cross-complementing protein 4

## **Preface**

Studying the profound biological pathways in the cell will open the gates into more precise diagnosis/therapy as a consequence. Delayed diagnosis and insufficient therapies, accompanying side effects, are the results of the current approach for numerous diseases.

NHEJ machinery as an example of a molecular pathway, fixes DSBs and keeps the homeostasis of the cell. Although, the NHEJ process is not fully understood. Further research is required to identify all proteins involved in the pathway, as well as other elements that can influence DNA repair efficiency.

Here, in Oksenysh lab at IKOM, NTNU, we put our efforts to elucidate the roles of molecules involved in NHEJ DNA repair system in the cell. We are challenged by the need for better diagnostics and therapies for the disorders related to inefficient DNA repair, which include immunodeficiency, as well as specific malignancies.

During recent years, discoveries in DNA repair and immunology were recognized by the Nobel committee and several other prestigious international awards. For me, it indicates that our research is in line with the needs of our society. It is my honor to perform research and discover new biological aspects of DNA repair during my MSc project. I believe that my results will add to the existing knowledge of biomedicine and will be valuable for society.



## 1. Introduction

All of the living organisms are exposed to DNA double-strand breaks (DSBs), caused by exogenous genotoxic stresses (such as Ultraviolet radiation, UV) or endogenous biological processes such as V(D)J recombination. DNA DSBs are described as the most toxic type of DNA lesion and need to be fixed to allow the continuation of cellular life. Henceforth, Homologous recombination (HR) and Non-homologous end joining (NHEJ) repair systems are two major molecular pathways that deal with DSBs [1-3].

However, there are other DNA repair machinery, such as Single-strand annealing (SSA), to fix DSBs. SSA repairs DSBs by annealing the tandem repeat sequences around DSB which results in the elimination of one of the repeat sequences [4].

While NHEJ can be activated at any phase of the cell cycle, HR functions only in S/G2 (Synthesis phase/ Gap 2 phase) phases [3]. Thereby, NHEJ is the major repair system in mammalian cells. NHEJ pathway involves various proteins. Some that are necessary for all DNA repair procedures are called core NHEJ factors, and some that are required for specific DSBs and more complex stabilization are called accessory factors [5].

DSBs activates NHEJ pathway, subsequently. Core elements Ku70 and Ku80 form a heterodimer structure and associate with DSBs location. Attachment of Ku70/80 facilitates the recruitment of downstream core factors including X-ray repair cross-complementing 4 (XRCC4), DNA ligase 4 (Lig4) and XRCC4-like factor (XLF) [3, 6-8].

Lig4 joins single-strand breaks (SSBs) in a double-stranded polydeoxynucleotide in an ATP-dependent reaction. To enhance the joining activity of Lig4, XRCC4 form the XRCC4-Lig4 complex by binding to DNA and Lig4. Meanwhile, XLF serves as a bridge between XRCC4 and other NHEJ elements located at DNA ends [3, 6-8].

On the other hand, a number of accessory NHEJ factors are required for the particular DNA end processing. Parologue of XRCC4 and XLF (PAXX), Modulator of retroviral infection (Mri/Cyren), DNA-dependent protein kinase catalytic subunit (DNA-PKcs) and Artemis are examples of the accessory factors. PAXX functions as a scaffold to stabilize the KU heterodimer and promotes the assembly of NHEJ machinery [9, 10]. Mri is a regulator of DNA repair system by inhibition of NHEJ during S and G2 phases [5, 11].

Among NHEJ accessory factors, DNA-dependent protein kinase catalytic subunit (DNA-PKcs) assembles a holoenzyme with Ku heterodimer and phosphorylates most NHEJ elements [9,

12]. Phosphorylated Artemis process the joining DNA before end ligation. Artemis by its endo/exonuclease activity opens hairpin-sealed ends and prepares DNA ends for further DNA repair procedure (Figure 1) [3, 13].

To accomplish a proper DNA repair, the DNA damage response (DDR) pathway operates in parallel with NHEJ. MRN complex plays a key role in DDR pathway and is involved in the initial processing of DSBs. MRN that is constructed by Mre11, Rad50 and NBS-1 subunits, binds to the DNA lesion site. Furthermore, NBS-1 subunit creates a bridge among DNA and nuclear protein kinase, ATM. Concomitantly with ATM activation, a series of involved repair proteins adhere to DSB sites.

DDR network continues with phosphorylation of histone protein H2AX (histone family member X), Brca1 (Breast cancer type 1 susceptibility protein), Chk2 (Checkpoint kinase 2), and p53. Activated H2AX arranges the chromatin structure to provide the following DDR events. Thenceforth, Chk2 arrests the cell cycle at G2 phase and phosphorylates p53. Activated p53 acts with DNA motif that results in the expression of required repair proteins (Figure 2) [14, 15].

**Figure 1**

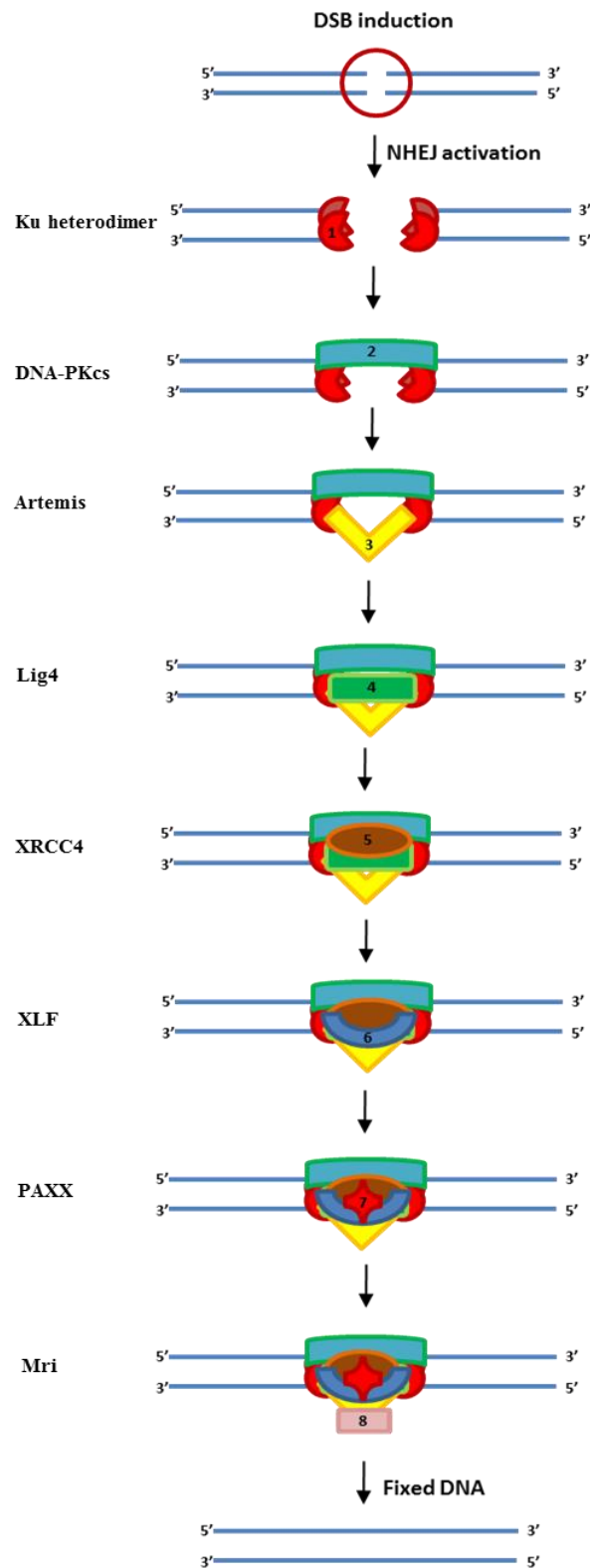


**Figure 1.** Schematic assembly of NHEJ machinery. Ku heterodimer (1) recognizes and binds to DNA breakage. DNA-PKcs (2) phosphorylates downstream elements. Artemis (3) cut the overhangs and supply DNA end ligation by Lig4 (4). XRCC4 (5) functions as the bridge between DNA and Lig4. The cooperation among XLF (6) and PAXX (7), stabilizes the complex. Mri functions as the cell cycle regulator (8).

**Figure 2**

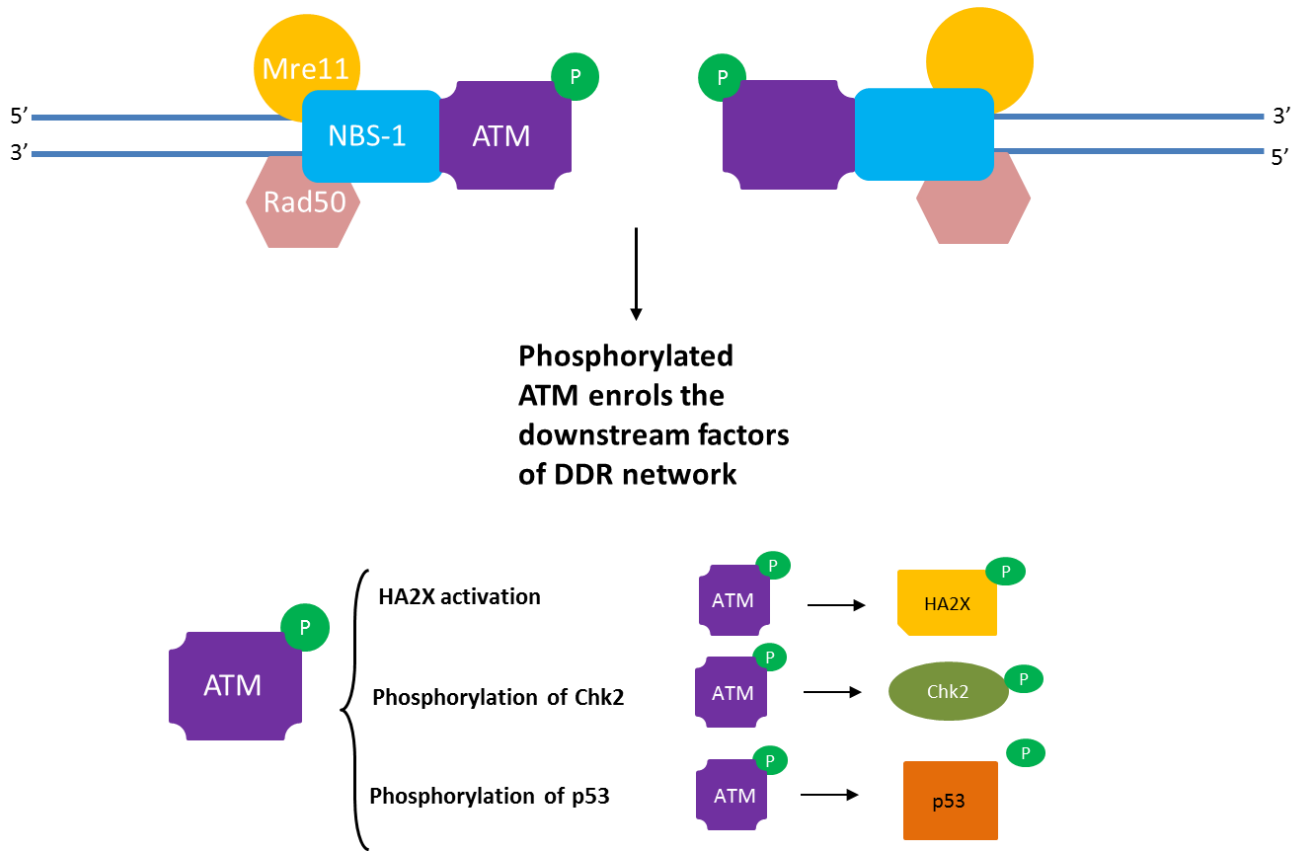


**Figure 2.** Functional links between the elements of the DDR repair network leads to the expression of repair proteins.

### 1.1 V(D)J recombination

The immune system functions against pathogens through innate and adaptive immunity approaches. The innate immunity deals with different pathogens (antigens) via a constant procedure. On the contrary, adaptive immunity differs from various antigens and develops throughout life. B and T lymphocytes are the two major functional elements of adaptive immunity.

Hematopoietic stem cells (HSCs) of bone marrow differentiate and generate B and T lymphocytes. B cell development remains in bone marrow, however, progenitor-T cells migrate to thymus for further development. Pre-pro-B cell is the first set of B cells in the B cell development process. Following, early pro-B cell is generated from pre-pro-B cell and differentiate to the late pro-B cell and then pre-B cell. Completed V(D)J recombination of antibody (BCR) heavy and light chain produce immature B cell from pre-B cell. In case of any association of immature B cell with stimuli, CSR performs different antibodies (Figure 3) [16].

**Figure 3**

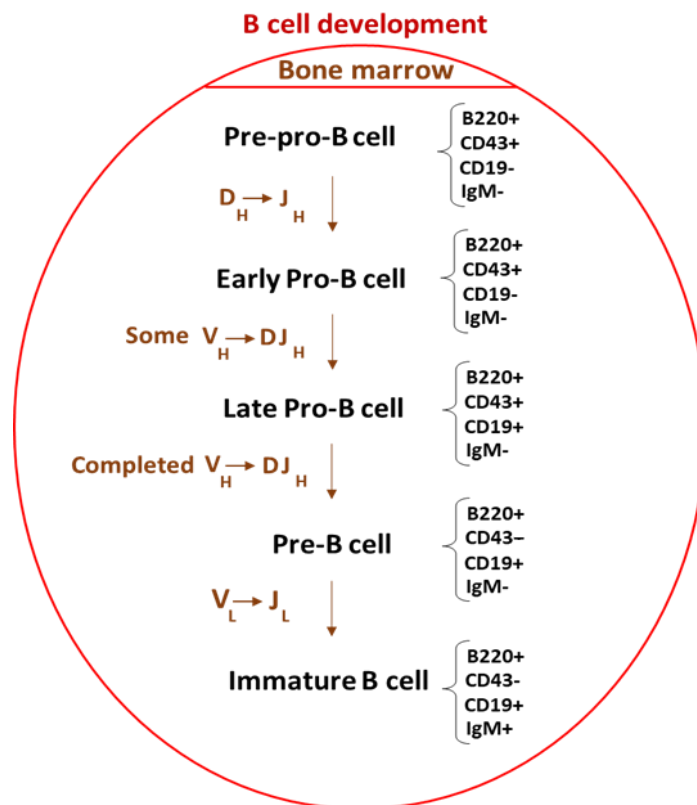


**Figure 3.** B cell development in the bone marrow. B cells have specific antigens at each stage of development [17].

B cells supply immunity by generating antibodies. Accordingly, produced antibodies locate within the B lymphocyte membrane and form B cell receptors (BCRs). An antibody composed of two immunoglobulin heavy chains (IgH) and two immunoglobulin light chains (IgL). Development of antibodies includes the rearrangement of *V*, *D* and *J* gene segments of heavy chain locus and *V* and *J* gene segments of light chain locus [16, 18].

HSCs in bone marrow produce progenitor T cells and then they migrate to the thymus to complete T cell development. In the thymus, progenitor T cells undergo a developmental process to mature and express T cell receptors (TCRs) to function. TCRs are divided into  $\alpha\beta$  and  $\gamma\delta$  T cell receptors and each one has a constant and a variable region. The majority of T cells acquire  $\alpha\beta$  TCR and less  $\gamma\delta$  type. *V*, *D* and *J* gene segments of  $\beta$  and  $\delta$  chains and *V* and *J* gene segments of  $\alpha$  and  $\gamma$  chains, experience V(D)J recombination through T lymphocyte development [16] (Figure 4).

**Figure 4**

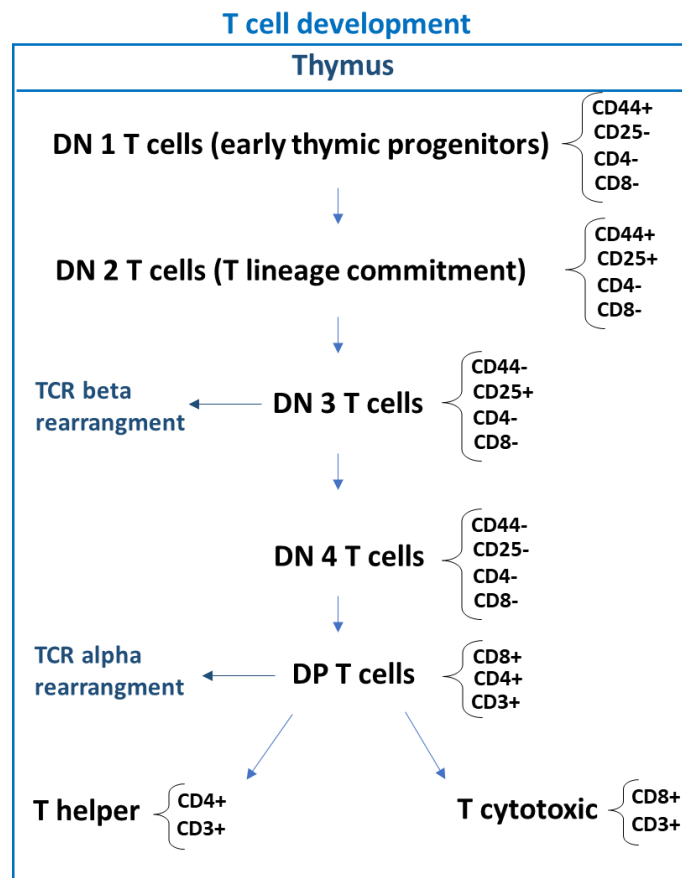


**Figure 4.** T cell development procedure. Generated progenitor T lymphocytes in bone marrow migrate to the thymus to finalize T cell development. T cell has specific antigens at every particular level of T cell development [17].

Distinct assembly and expression of *V*, *D* and *J* gene segments of B and T lymphocytes result in diverse BCR and TCR production that makes lymphocytes function specifically against various pathogens. V(D)J recombination is the event required to rearrange the gene segments. An antibody consists of heavy and light chains that each of them has constant (*C*) and variable regions (*V*). The gene that generates the heavy chain is located on chromosome 14 in humans and chromosome 12 in mice. While the responsible gene for light chain expression is placed on chromosome 22 (in case of kappa chain selection) or chromosome 2 (in case of lambda chain selection) in humans and on chromosome 16 in mice [19].

Antibody heavy chain gene includes *V* (variable), *D* (diversity), *J* (joining), and *C* (constant) gene segments (ordered respectively) (Figure 5). Moreover, the light chain gene consists of *V* (variable), *J* (joining), and *C* (constant) sections (ordered respectively) (Figure 7). V(D)J recombination assembles a different *V* gene segment with a distinct *D* and *J* gene segments that results in antibodies (BCRs) and TCRs with new heavy and light chains, for B and T lymphocytes [20].

**Figure 5**

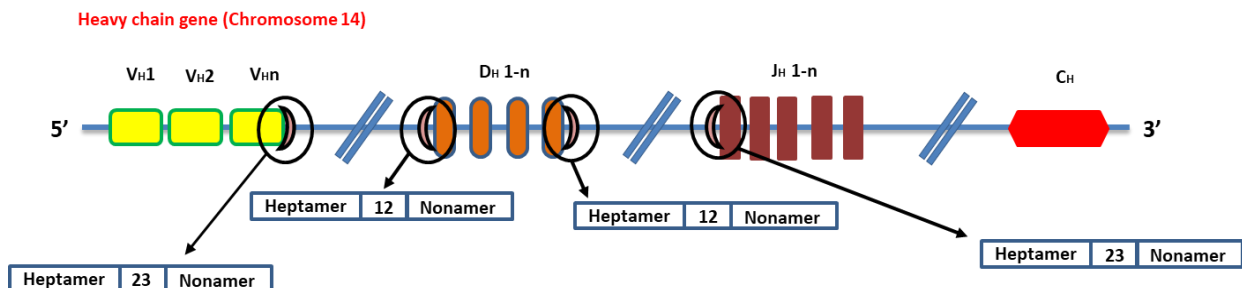


**Figure 5.** The organization of *V*, *D*, and, *J* gene segments in human IGH locus on chromosome 14.

There are signal sequences around the gene segments (*V*, *D*, and, *J*) called Recombination Signal Sequence (RSS). RSS is essential for initiating V(D)J recombination. RSS guides participating factors to assemble the proper and diverse gene segments. RSS composed of a Heptamer (conserved 7 nucleotides) in addition to a spacer region of 12 or 23 base pairs, plus a Nonamer (conserved 9 nucleotides) respectively (Figure 5) [21].

RSS is identified by a complex called recombination activating genes 1 and 2 (RAG1 and RAG2) proteins. RAG1/2 complexes rejoin the gene segments in a new order by generating

and then cleavage of DNA loops. New *V.D.J* sequence then binds to *C* region (Figure 6). Generated DNA nick between selected gene segments, repairs by NHEJ system that opens the hairpin-sealed DNA ends and ligates separated DNA strands. The same pathway is selected for the antibody light chain gene, while, there is no *D* gene segment and light chain is either kappa (if recombination occurs in chromosome 22) or lambda (if recombination occurs in chromosome 2) (Figure 7) [22].

TCR consists of alpha and beta chains, each contains Variable (V) and Constant (C) sections. T cells bear the same mechanism for TCR assembly to generate diversity. TCR alpha and beta chain gene segments carry out an orientation that is broadly homologous to the BCR gene segments that is  $V > D > J$  for beta chain and  $V > J$  for alpha chain [19].

TCR beta gene segments are located on chromosome 6 in mice and on chromosome 7 in humans. Notably, chromosome 14 consists of TCR alpha chain gene segments in both humans and mice [23, 24].



**Figure 6**

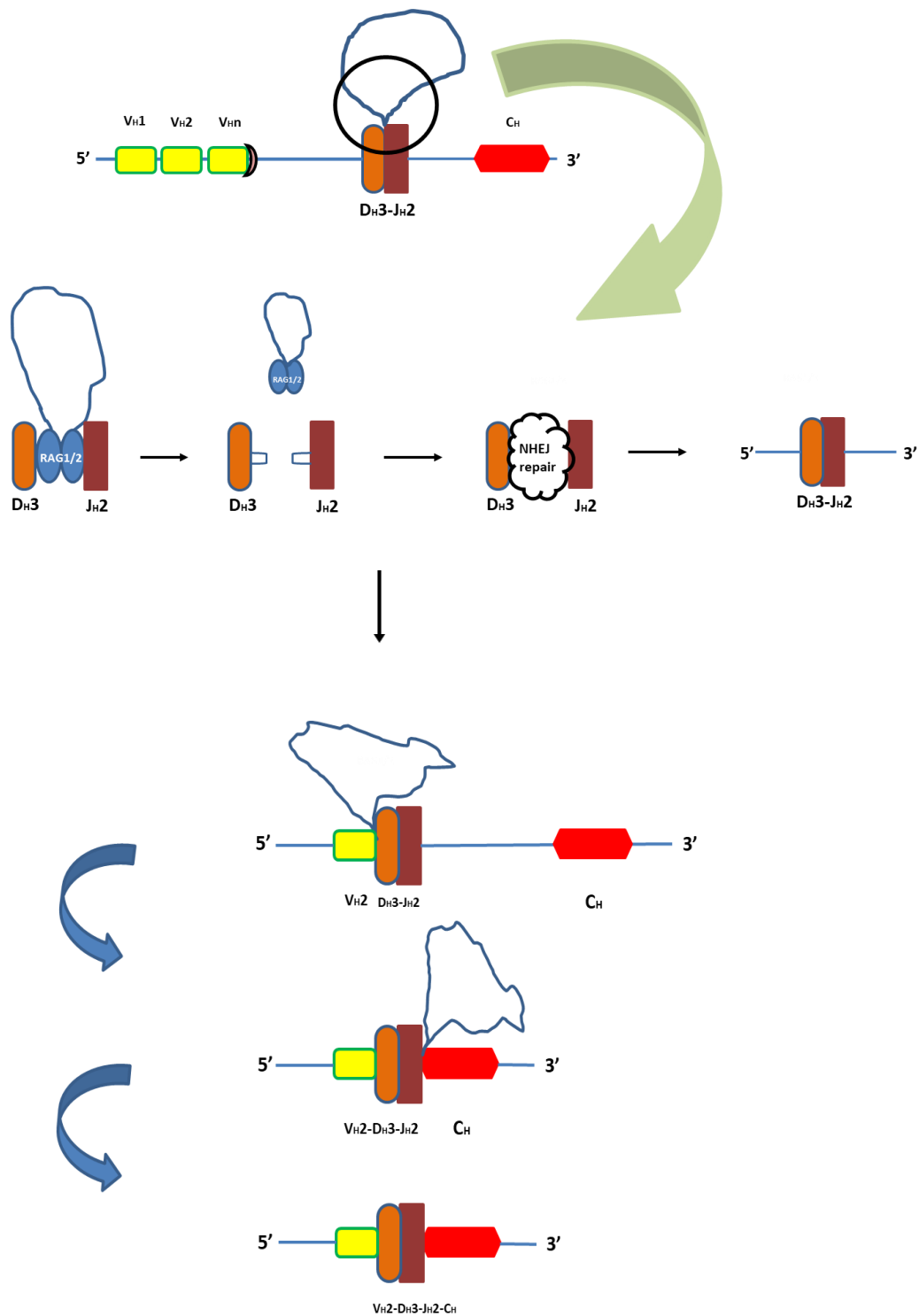


**Figure 6.** V(D)J recombination, followed by NHEJ repair machinery. RAG 1/2 protein recognizes RSS in various segments and connects the selected segments by introducing DNA loops. The gene segment *J* to *D* and *DJ* to *V* is the orientation of the V(D)J recombination in the heavy chain of the BCR and beta chain of the TCR.

**Figure 7**

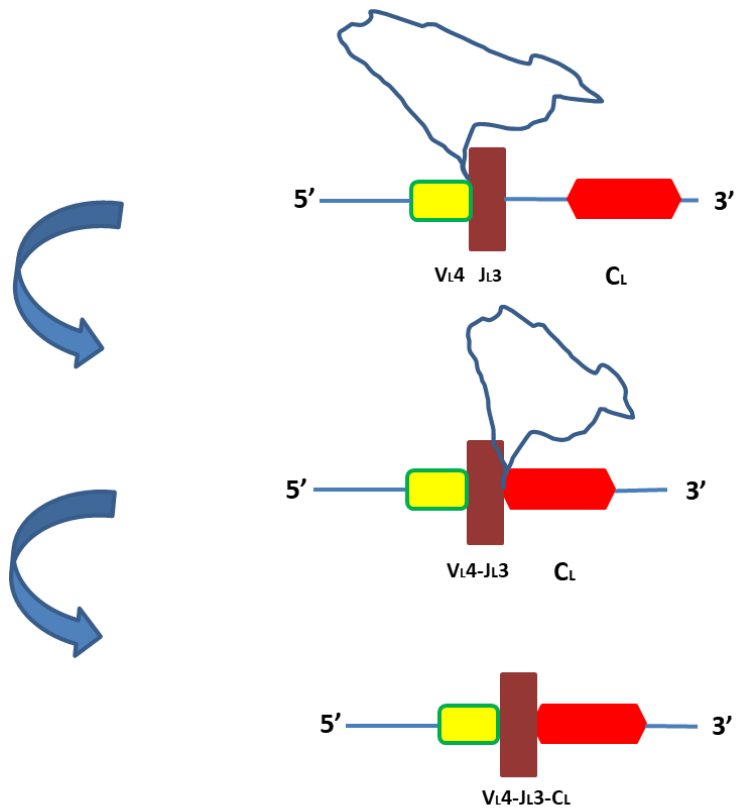


**Figure 7.** V(D)J recombination in the BCR light chain on B cells and TCR alpha chain on T cell has the same process.

## 1.2 Class switch recombination

A specific physiological mechanism in B cells is class switch recombination (CSR). CSR makes B cells capable to establish diverse isotypes of immunoglobins with high affinity by switching the C sections of different antibody heavy chain regions. Interaction of B cell with T helper cell or cytokines triggers CSR that results in B cell maturation [19].

B cell maturation followed by the activation of transcription factors (TFs). Activated TFs attach to Switch regions (S). Switch regions are Guanin/Cytosine rich tandem repeats at upstream of C gene segments (chromosome 14 in humans and chromosome 12 in mice). The position of C gene segments in mice is: 5' - (S $\mu$ ) C $\mu$  - C $\delta$  - (S $\gamma$ 3) C $\gamma$ 3 - (S $\gamma$ 1) C $\gamma$ 1 - (S $\gamma$ 2b) C $\gamma$ 2b - (S $\gamma$ 2a) C $\gamma$ 2a - (S $\epsilon$ ) C $\epsilon$  - (S $\alpha$ ) C $\alpha$  - 3' and in humans is: 5' - (S $\mu$ ) C $\mu$ -C $\delta$ -(S $\gamma$ 3) C $\gamma$ 3-(S $\gamma$ 1) C $\gamma$ 1-(S $\psi$  $\epsilon$ ) C $\psi$  $\epsilon$  - (S $\alpha$ 1) C $\alpha$ 1 - (S $\psi$  $\gamma$ ) C $\psi$  $\gamma$  - (S $\gamma$ 2) C $\gamma$ 2 - (S $\gamma$ 4) C $\gamma$ 4 - (S $\epsilon$ ) C $\epsilon$  - (S $\alpha$ 2) C $\alpha$ 2 - 3' [25].

Interaction of TFs and S regions recruits RNA Pol II and this enzyme opens DNA strands. Meanwhile, Activation-induced cytosine deaminase (AID) enzyme starts deamination of cytosines and converts them into uracil. Then, Apurinic/aprimidinic endonuclease 1 (APE1) and Uracil-DNA glycosylase (UNG or UDG) generate DNA breaks within or nearby S regions [19].

The space sequences among the introduced breaks will remove and then NHEJ machinery joins DNA ends that results in switched isotype of the antibody with the same affinity (Figure 8).

Figure 8

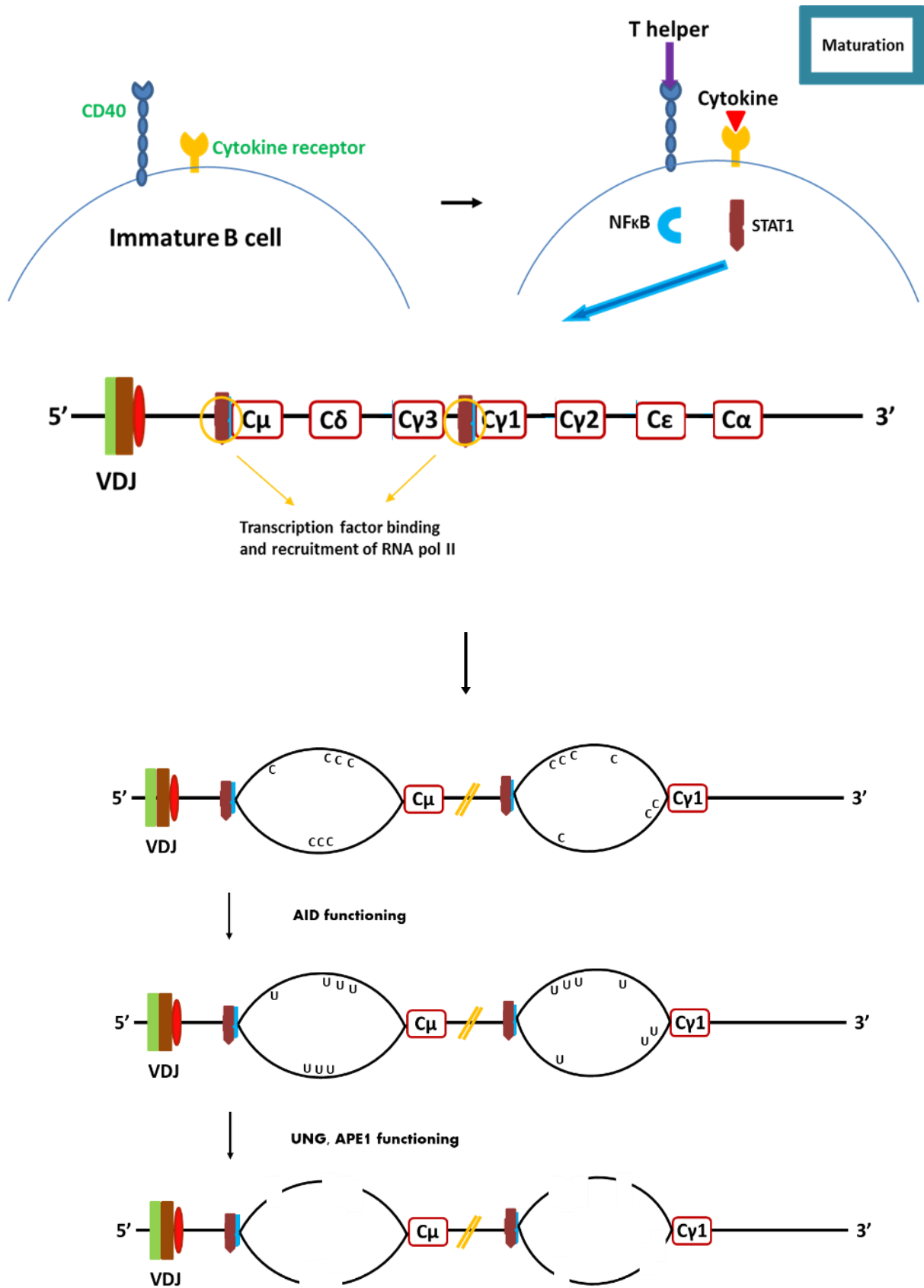
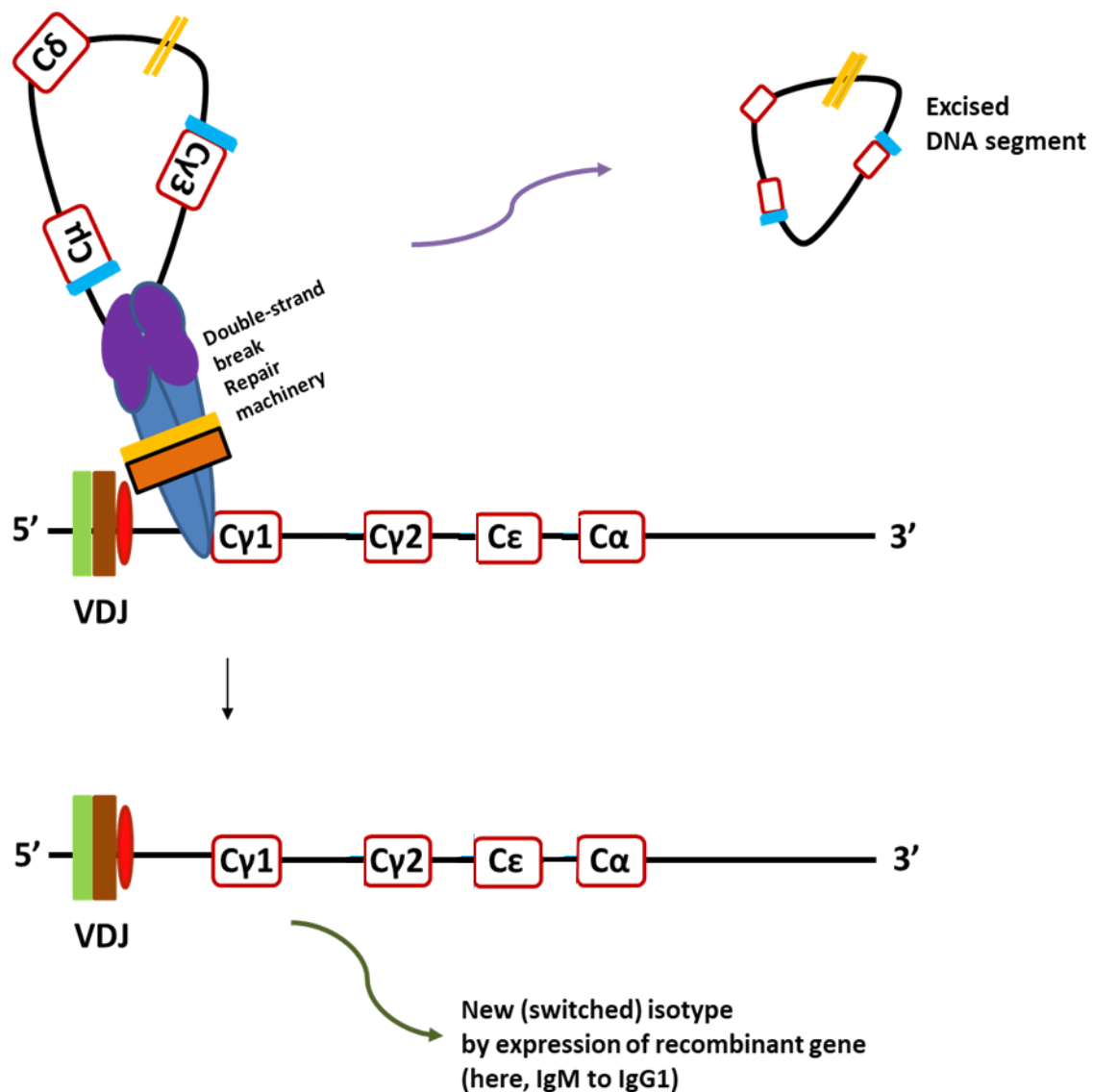


Figure 8. The maturation of B cell is followed by the activation of transcription factors.

The interconnection of a TF to a specific *S* region, determines that IgM or IgD would be switched to which isotype of immunoglobulin. For instance, in the case of IgM to IgG switch recombination, TFs bind to  $S_{\mu}$  and  $S_{\gamma}$ . CSR mechanism starts and after generating DNA DSBs, NHEJ factors meet  $S_{\mu}$  and  $S_{\gamma}$  ends. The new oriented gene would be ready to express IgG (Figure 9) [19].

**Figure 9**



**Fig 9.** RNA pol II opens *S* regions at the upstream of the selected *C* gene segments. CSR followed by AID, UNG, and APE1 functions. NHEJ joins DNA ends.

### 1.3 B and T cell development associated diseases in humans

There are examples of disorders related to B and T cell development in humans (Table 1). Noticeably, mutations in NHEJ repair system cause ablated V(D)J recombination that leads to failure in B and T cell development. RAG1/2 protein insufficiency in humans leads to Omenn syndrome (OS) which is characterized by a lack of circulating B cells [26]. Also, mutation in genes encoding ARTEMIS and Lig4 proteins in humans cause severe combined immunodeficiency (SCID) [27-29]. On the other hand, the autosomal recessive form of Hyper-IgM syndrome in humans is an example of CSR associate disease that cause by defects in AID [30].

There are different diagnosis/treatment methods to increase the life expectancy of the patients dealing with the mentioned abnormalities and immunodeficiencies in general. For instance, flow cytometry analysis of lymphocytes in peripheral blood is a diagnostic method and bone marrow transplantation is a possible treatment [31, 32]. Although, the current approaches are incomplete to deal with immunodeficiencies. Early-life infection-related mortalities in the patients decline that we need more precise diagnosis to anticipate immunodeficiencies. Following, identifying the genetic etiology of immune dysfunction diseases will make us eligible for target therapies [33].

Thus, studying NHEJ core and accessory factors in mice, help us to understand the profound mechanisms in B and T cell development-related diseases. Mice lacking *Xlf* possess normal or only have modest immunodeficiency [34-37]. While, inactivation of other NHEJ factors such as *Ku70*, *Ku80*, *Artemis* and *Dna-pkcs* cause blockage of B and T cell development in mice [38-41]. Notably, *Lig4<sup>-/-</sup>* and *Xrcc4<sup>-/-</sup>* single knock out mice are embryonically lethal [42, 43].

On the other hand, mice lacking *Paxx* or *Mri* have normal B and T cell development [9, 34-36, 44-47]. It was explained that XLF deficiency in mice is compensated by other DNA repair factors [6, 35, 46, 48]. Importantly, some factors of DNA repair have overlapping roles that makes it more challenging to study. Genetic interaction (GI) is a useful approach to identify more factors involved in DNA repair and B and T cell development. GI reveals that it is possible to observe a surprising phenotype caused by the mutation in two genes, which is different from each mutation's result. Studying the outcome phenotype after applying the mutations, portrays the connection among different genes [49, 50].

Noticeably, *Xlf<sup>-/-</sup>Paxx<sup>-/-</sup>* double deficient mice are lethal that shows functional redundancy between *Xlf* and *Paxx* in mice [35, 36, 51]. Inactivation of single or both alleles of *Trp53* rescues embryonic lethality and allows postnatal survival [35, 46]. *Xlf<sup>-/-</sup>Paxx<sup>-/-</sup>Trp53<sup>+/-</sup>* mice have severe immunodeficiency with lack of mature B and T cells in spleen and thymus [35]. Although, it is not clear whether B lymphocytes mature normally via V(D)J recombination in bone marrow and die before migration to the periphery, or V(D)J recombination is blocked at the primary stage of B cell development in bone marrow of *Xlf<sup>-/-</sup>Paxx<sup>-/-</sup>Trp53<sup>+/-</sup>* mice.

While mice lacking *Mri* or *Paxx* possess normal lymphocyte development, *Dna-pkcs<sup>-/-</sup>* mice are live-born and have SCID phenotype [5, 9, 34-36, 41, 44, 47, 51]. Studying the genetic interaction between *Mri* and *Dna-pkcs* in addition to *Mri* and *Paxx* can reveal whether they interact genetically or not, in aspects of B and T cell and general development in mice.

<b>Deficiency</b>	<b>Symptoms</b>	<b>Reason</b>
RAG1/2	Lack of circulating B cells	V(D)J recombination blockage
Lig4	Severe combined immunodeficiency (SCID)	No ligation during NHEJ
ARTEMIS	Severe combined immunodeficiency (SCID)	Abnormal NHEJ
AID	Hyper level of IgM	Ablated CSR

**Table 1.** Example of diseases related to deficient B and T cell development in humans.

## 2. Hypotheses and research aims

My hypotheses are:

- 1) Lack of B and T cells in *Xlf<sup>-/-</sup>Paxx<sup>-/-</sup>Trp53<sup>+/-</sup>* mice is rooted in bone marrow and thymus caused by NHEJ blockage at the early stage of lymphocyte development.
- 2) *Mri* and *Dna-pkcs* genes have overlapping functions and interact genetically, including aspects of B and T cell development and general mouse phenotype.
- 3) *Mri* and *Paxx* genes are functionally redundant and interact genetically regarding B and T cell development and general mouse phenotype.

To verify my hypotheses experimentally, I developed the following aims:

- 1) Analysis of the lymphoid organs of *Xlf<sup>-/-</sup>Paxx<sup>-/-</sup>Trp53<sup>+/-</sup>* mice to certify the previous observations.
- 2) Examination of the bone marrow of *Xlf<sup>-/-</sup>Paxx<sup>-/-</sup>Trp53<sup>+/-</sup>* mice to notice the early-stage B cell development of the deficient mice.
- 3) Generation of *Mri<sup>-/-</sup>Dna-pkcs<sup>-/-</sup>* mice and then, analysis of B and T lymphocyte development in the deficient mice.
- 4) Generation of *Mri<sup>-/-</sup>Paxx<sup>-/-</sup>* mice and then, analysis of B and T lymphocyte development in the deficient mice.



### 3. Material and Methods

#### 3.1 Mouse models

All the experiments involving mice were performed according to the protocols approved by the Norwegian University of Science and Technology (NTNU). *Xlf*<sup>+/-</sup> [37], *Paxx*<sup>+/-</sup> [9], *Mri*<sup>+/-</sup> [5] (Appendix A), *Dna-pkcs*<sup>+/-</sup> [41], *Trp53*<sup>+/-</sup> [52] mice were described previously. Primer sequences for genotyping and expected amplicons are provided in Appendix B. Breeding of different genotypes is mentioned in the results section.

#### 3.2 Genotyping

##### 3.2.1 DNA extraction and Polymerase Chain Reaction (PCR)

To extract DNA from mice ear samples, 2% Proteinase K (20 mg/ml) (Cat#AM2546, Ambion™, Waltham, Massachusetts, United States) and 98% DNA lysis buffer (10mM Tris pH 9.0, 1M KCl, 0.4% NP-40, 0.1% Tween20) were added to the samples and then incubated overnight at 56°C, 450rpm in Thermoblot mixer device (No. 5355 26163, Eppendorf AG, Hamburg, Germany). Furthermore, the samples were incubated at 95°C for 30 minutes and centrifuged at 15 000 rpm for 15 minutes.

The concentration of the extracted DNA was measured by the Nanodrop® ND-1000 Spectrophotometer (Thermo Scientific, Waltham, Massachusetts, United States). Samples were diluted to get the final DNA concentration that is approximately 50ng/μL. The PCRs were run with 50ng DNA in a reaction volume of 25μL, utilizing the GoTaq® G2 Green Master Mix (Cat#M7823, Promega, Madison, USA) and performed in the 2720 Thermal Cycler (Applied Biosystems™, Foster City, California, United States). PCR programs are provided in Appendix C.

##### 3.2.2 Electrophoresis

Agarose gels were prepared to separate amplified DNA sequences according to the size and composed, GelRed™ Nucleic Acid Gel Stain (Cat# 41003, 10 000x in water, Biotium, Fermont, California, USA), 0.8% SeaKem® LE Agarose (Cat#50000, Lonza, USA), and Tris-Borate-EDTA (TBE) buffer (pH 8.4; 89mM Tris; 89mM Boric Acid; 2mM EDTA). The sample volume loaded on the gels was 10μL and for reliability, WT (wildtype allele), mutant

(allele), and ddH<sub>2</sub>O (double distilled water) controls were considered in all assays. Then, gel electrophoresis was run in TBE buffer chamber at 124V for 75 minutes (100ml gels).

To supply DNA ladder and tracking dye in the gel, Quick-Load® 100bp DNA Ladder (Cat#N0467S New England Biolabs® Inc, Massachusetts 1938 United States) and Orange G 5x ~50bp (15% glycerol; 0.2% Orange G dye, ddH<sub>2</sub>O) were used respectively. Then gels were visualized and pictured by the Gel Logic 200 Imaging System (KODAK, United States).

### **3.3. Count of cells isolated from the lymphoid organs**

All the analyzed mice were 5 to 8 weeks old, females and males pooled together. In the beginning, spleens, thymi and femora were isolated from mice. Spleens and thymi were weighed on a Mettler Toledo AG240 DeltaRange weight (Mettler-Toledo GmbH, Laboratory & Weighing Technologies, CH-8606 Greifensee, Switzerland). Isolated organs were placed in petri dishes containing 10mL of 1X Phosphate-buffered saline (PBS) (Cat#BR0014G Oxiod, Hampshire, England). Needles with syringes were utilized to extract bone marrow from the femora. A plunger of a syringe was applied to mash the spleens, thymui and bone marrow tissue to release the cells into PBS. Cell suspensions were filtered through 40µm Fisherbrand™ Sterile Cell Strainers (Cat#22-363-547, Fisher Scientific, Hampton, New Hampshire, United States) into 50ml conical centrifuge tubes and then centrifuged at 2000rpm for 5 minutes at 4°C.

Supernatants were out and pellets were resuspended in 1ml of Red Blood Cell (RBC) Lysis Buffer Hybri-Max™ (Cat#R7757, Sigma-Aldrich, St. Louis, Missouri, United States) gently and incubated for 5 minutes at RT to lyse erythrocytes. Thereafter, cells were diluted with 1X PBS to supply the optimal counting range for the cell counter ( $1 \times 10^4 - 1 \times 10^7$  cells/mL). Cells were then diluted in Trypan Blue Stain 0.4% (Cat#T10282 Invitrogen™ Carlsbad, California, United States) and added into Countess™ Cell Counting Chamber Slides (Cat#C10228, Invitrogen™, Waltham, Massachusetts, United States) and counted through Countess II FL Automated Cell Counter (Cat#AMQAF1000, Invitrogen™, Waltham, Massachusetts, United States).

### **3.4. Cell staining for Flow Cytometry analysis**

After cell counting, to get a final concentration of  $2.5 \times 10^6$  cells/mL for each sample, a certain amount of cells were added into 1.5ml tubes. Hereafter, cell suspensions were spun down (2000rpm for 5 minutes at 4°C) and diluted with 100µl cold 1X PBS-5% Fetal bovine serum (FBS) (Cat#F7524, Sigma Life Science, St. Louis, Missouri, United States). The process is followed by adding 1µl fluorochrome-conjugated antibodies (applied antibodies for flow cytometry are described in Table 2) into each 1.5ml tube and gently mixing. After 30 minutes of incubation in darkness at 4°C, cells were washed with 500µl cold 1X PBS-5%FBS and centrifuged at 2000rpm for 5 minutes at 4°C. Supernatants (500µl from each 1.5 ml tube) were discarded and cell pellets were resuspended in 500µl cold 1X PBS-5%FBS.

The concluding cell suspensions were transferred into into Falcon™ Round-bottom polystyrene tubes (Cat#352054, Corning™, NewYork, United States) and were ready for flow cytometry analysis acquired on a BD FACSCanto™ Cytometer (Cat#951312350, BD Biosciences, Qume Drive, San Jose, United States). Single stained splenocytes/thymocytes (CD3+/CD19+/CD4+/CD8+/B220+/IgM+/CD43+) were employed as compensation controls to correct the data.

Obtained data was further analyzed performing the FlowJo® V10 software (FlowJo LLC, New Jersey, USA).

Antibody	Fluorochrome Conjugate	Dilution	Catalog#	Supplier
Hamster Anti-Mouse CD3e	FITC	1:100	561827	BD Pharmingen™
Anti-Mouse CD19	PE/Cy7	1:100	115520	Biolegend
Rat Anti-Mouse CD4	PE-Cy7	1:100	552775	BD Pharmingen™
Rat Anti-Mouse CD8a	PE-Cy™5	1:100	553034	BD Pharmingen™
Rat Anti-Mouse CD45R/B220	APC	1:100	553092	BD Pharmingen™
Rat Anti-Mouse IgM	PE-Cy™7	1:100	552867	BD Pharmingen™
Rat Anti-Mouse CD43	FITC	1:100	561856	BD Pharmingen™

**Table 2.** Antibodies used for flow cytometry analysis. The given dilutions were used for  $2,5 \times 10^6$  cells.

### 3.5 Statistics

GraphPad Prism 8 (La Jolla, California, USA) was utilized according to statistical analysis of body weight, spleen weight, thymus weight, cell counts and proportions of B and T lymphocytes for the various genotypes. Besides, the one-way analysis of variance (ANOVA) formula was applied to all groups of variables.

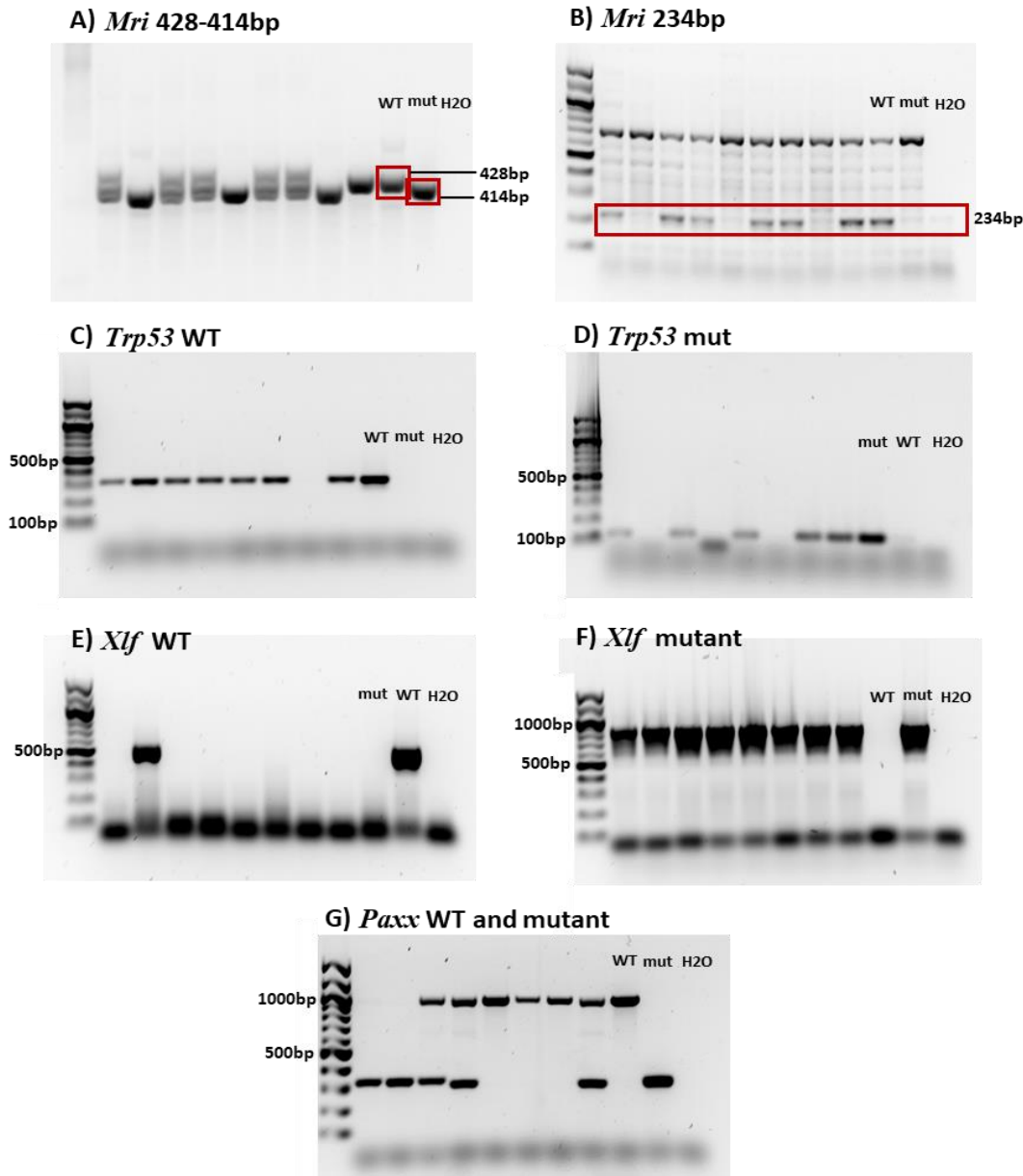
## 4. Results

### 4.1 Genotyping

All mice selected for breeding, organ isolation, cell counting and flow cytometry analysis were identified by genotyping PCR and gel electrophoresis. DNA was extracted from ear samples. Examples of all PCR experiments run during this project are illustrated in Figure 10. For accuracy, WT (allele), mutant (allele) and ddH<sub>2</sub>O controls were performed in all PCR assays.

Examples of *Xlf<sup>-/-</sup>Paxx<sup>-/-</sup>Trp53<sup>+/-</sup>* and *Mri<sup>-/-</sup>Paxx<sup>-/-</sup>* mice characterized by PCR are shown in Figure 11.

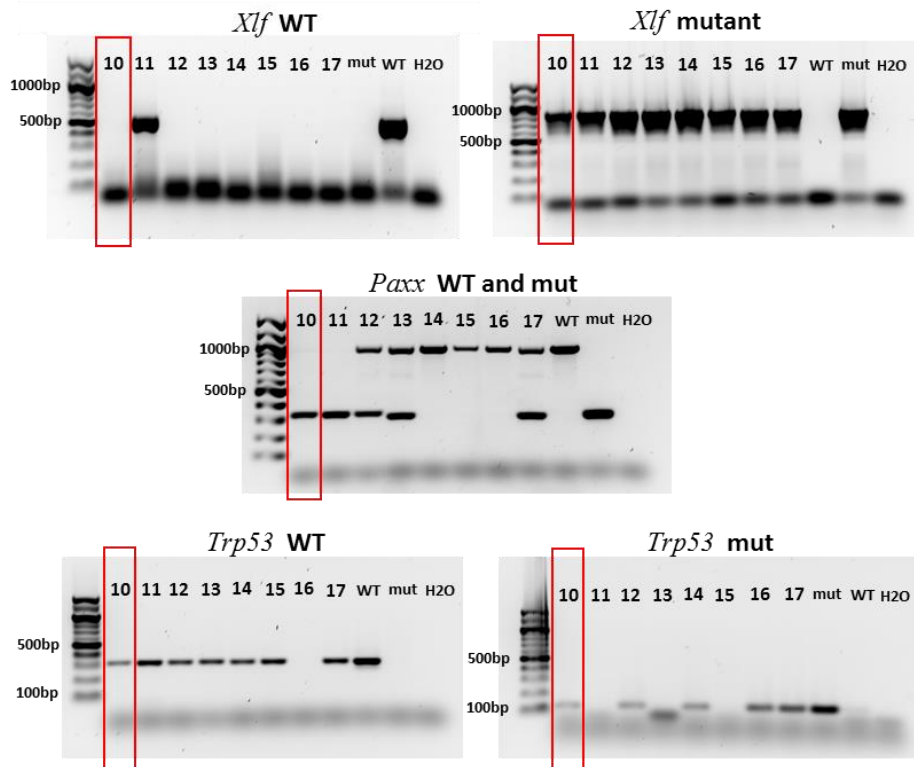
Figure 10



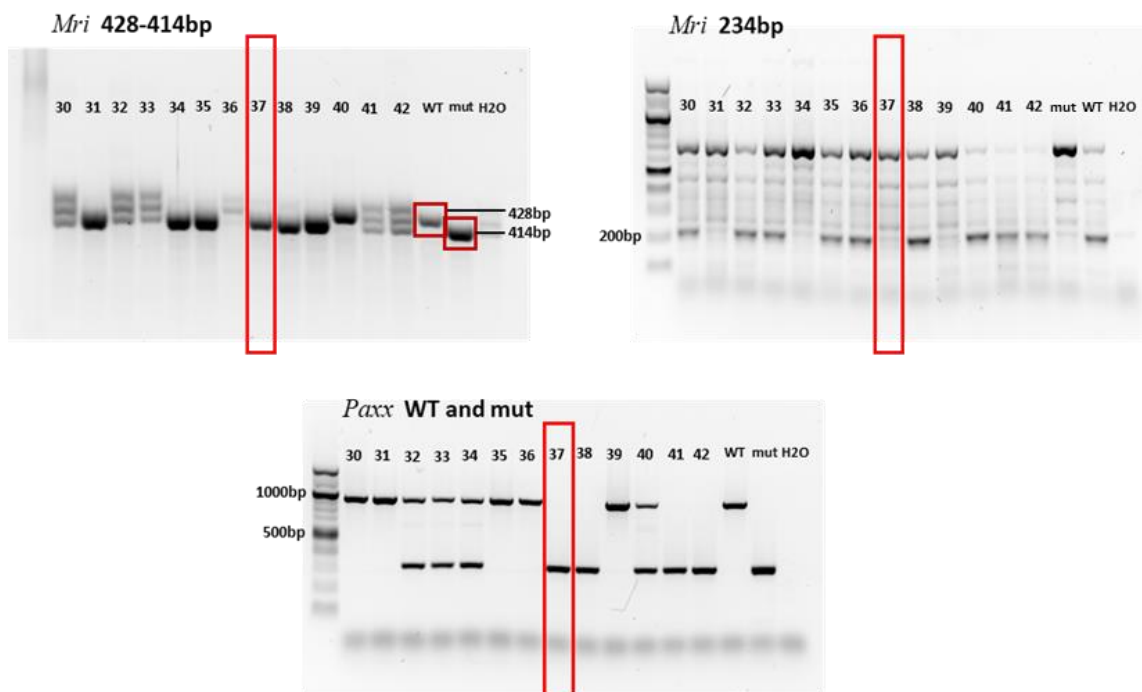
**Figure 10.** Illustration of genotyping PCR to detect WT and mutant *Mri*, *Trp53*, *Xlf* and *Paxx* genes, including WT (allele), mutant (allele) and ddH<sub>2</sub>O controls. **A)** *Mri* 428-414bp. Bands with 428bp length represent WT allele and bands at 414bp are null mutations (single band at 428bp: *Mri*<sup>+/+</sup>, one band at 428bp and one at 414bp: *Mri*<sup>+/-</sup>, single band at 414bp: *Mri*<sup>-/-</sup>). **B)** *Mri* 234bp. PCR was run and resulted band at 234bp represents that WT allele is present (*Mri*<sup>+/+</sup> or *Mri*<sup>+/-</sup>), and no band shows that only null mutation alleles are present (*Mri*<sup>-/-</sup>). Since the distance between the bands at 428bp and 414bp is only 14bp and 234bp PCR does not differentiate between WT and heterozygote *Mri*; both PCRs are applied to certify the genotyping result. **C)** *Trp53* WT. Bands correspond to *Trp53* WT allele (321bp). **D)** *Trp53* mutant. Bands correspond to *Trp53* mutant allele (110bp). **E)** *Xlf* WT. Bands represent the *Xlf* WT allele (650bp). **F)** *Xlf* mutant. Bands represent the mutant allele (950bp). **G)** *Paxx* WT and mutant. The upper bands serve the WT allele (965bp) and the lower bands portray the mutant allele (either 329bp, 312bp or 295bp bands. The reason is that three independent *Paxx* knock out sub-lines were used).

Figure 11

A) Example of *Xlf*<sup>-/-</sup>*Paxx*<sup>-/-</sup>*Trp53*<sup>+/-</sup> mouse



B) Example of *Mri*<sup>-/-</sup>*Paxx*<sup>-/-</sup> mouse



**Figure 11.** Example of *Xlf*<sup>-/-</sup>*Paxx*<sup>-/-</sup>*Trp53*<sup>+/-</sup> and *Mri*<sup>-/-</sup>*Paxx*<sup>-/-</sup> mice. **A)** Sample number 10, highlighted in Figure 11-A, represents *Xlf*<sup>-/-</sup>*Paxx*<sup>-/-</sup>*Trp53*<sup>+/-</sup> genotype (mutant allele band for *Xlf* and *Paxx* genes and both WT and mutant allele bands for *Trp53* gene are marked). **B)** Sample number 37, signified in Figure 11-B, corresponds to *Mri*<sup>-/-</sup>*Paxx*<sup>-/-</sup> genotype (only one band in 414bp (mutant allele) and no band in 234bp in *Mri* gene and only lower band (mutant allele) in *Paxx* gene).

#### 4.2 Immune system development in *Xlf<sup>-/-</sup>Paxx<sup>-/-</sup>Trp53<sup>+/-</sup>* mice

According to the previous studies, inactivation of one or both alleles of *Trp53* gene rescues embryonic lethality, caused by *Xlf<sup>-/-</sup>Paxx<sup>-/-</sup>* double knock out [5, 35]. Analyzed mice were generated from the crossbreeding of *Xlf<sup>-/-</sup>Paxx<sup>+/-</sup>Trp53<sup>+/-</sup>* mice. To perform my first and second research aims, I investigated 54 mice in total. The dispersal of the expected and analyzed mice is outlined in Table 3. Analyzed mice were generated from *Xlf<sup>-/-</sup>Paxx<sup>+/-</sup>Trp53<sup>+/-</sup>* parents. Considering the embryonic lethality of *Xlf<sup>-/-</sup>Paxx<sup>-/-</sup>* double knock out, no *Xlf<sup>-/-</sup>Paxx<sup>-/-</sup>Trp53<sup>+/-</sup>* mouse was observed that is marked in red color in Table 3.

Genotype	Number of offspring, P30	Expected 1:2:1:2:4:2:1:2:1
<i>Xlf<sup>-/-</sup>Paxx<sup>+/+</sup>Trp53<sup>+/+</sup></i>	5	3.37
<i>Xlf<sup>-/-</sup>Paxx<sup>+/+</sup>Trp53<sup>+/-</sup></i>	6	6.74
<i>Xlf<sup>-/-</sup>Paxx<sup>+/+</sup>Trp53<sup>-/-</sup></i>	2	3.37
<i>Xlf<sup>-/-</sup>Paxx<sup>+/-</sup>Trp53<sup>+/+</sup></i>	7	6.74
<i>Xlf<sup>-/-</sup>Paxx<sup>+/-</sup>Trp53<sup>+/-</sup></i>	21	13.48
<i>Xlf<sup>-/-</sup>Paxx<sup>+/-</sup>Trp53<sup>-/-</sup></i>	5	6.74
<i>Xlf<sup>-/-</sup>Paxx<sup>-/-</sup>Trp53<sup>+/+</sup></i>	0	3.37
<i>Xlf<sup>-/-</sup>Paxx<sup>-/-</sup>Trp53<sup>+/-</sup></i>	6	6.74
<i>Xlf<sup>-/-</sup>Paxx<sup>-/-</sup>Trp53<sup>-/-</sup></i>	2	3.37
<b>Total</b>	<b>54</b>	<b>54</b>

**Table 3.** Inactivation of *Trp53* rescues embryonic lethality of *Xlf<sup>-/-</sup>Paxx<sup>-/-</sup>* mice. The number of thirty-day-old mice (P30) of the indicated genotypes is reported. Expected mendelian distribution is provided in the third column. Both parents had *Xlf<sup>-/-</sup>Paxx<sup>+/-</sup>Trp53<sup>+/-</sup>* genotype.

As discussed before, XLF has redundant functions with PAXX and upon inactivation of both genes, the mice die embryonically due to impairment in NHEJ pathway [5, 34-36, 44]. Embryonic lethality caused by *Xlf<sup>-/-</sup>Paxx<sup>-/-</sup>* deficiency is rescued by the mutation in one or both alleles of *Trp53* gene [5, 35, 46]. This allows us to study the overlapping functions of XLF and PAXX proteins. V(D)J recombination are blocked in *Xlf<sup>-/-</sup>Paxx<sup>-/-</sup>Trp53<sup>+/-</sup>* mice that results in immune system defects [35]. The further research question was to identify the reason for low B cell count in *Xlf<sup>-/-</sup>Paxx<sup>-/-</sup>Trp53<sup>+/-</sup>* mice. One option was the V(D)J recombination block and thus blockage at pro-B cell stage of development.

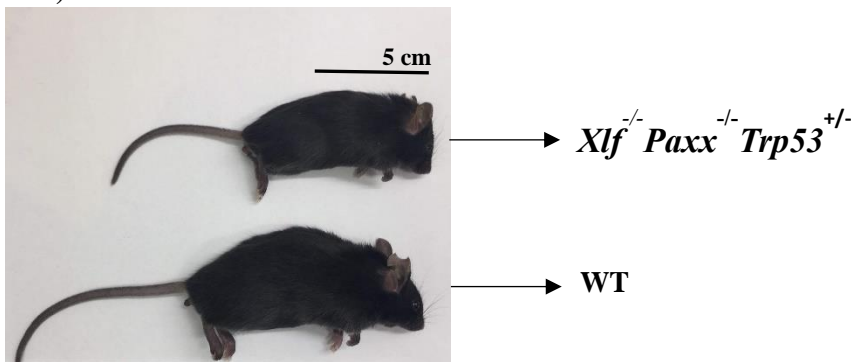


To answer this question and to verify the previous observation in *Xlf<sup>-/-</sup>Paxx<sup>-/-</sup>Trp53<sup>+/-</sup>* mice, I analyzed 9 *Xlf<sup>-/-</sup>Paxx<sup>-/-</sup>Trp53<sup>+/-</sup>*, 4 *Xlf<sup>-/-</sup>* and 7 WT mice. *Xlf<sup>-/-</sup>* mice were used as the single knock out control. *Paxx<sup>-/-</sup>* mouse was not available at the time of the experiment. However, PAXX-deficient mice possess WT phenotype [9, 34-36, 44, 51]. The weight of body, spleens and thymi were measured. Likewise, the number of splenocytes, thymocytes and bone marrow cells was recorded.

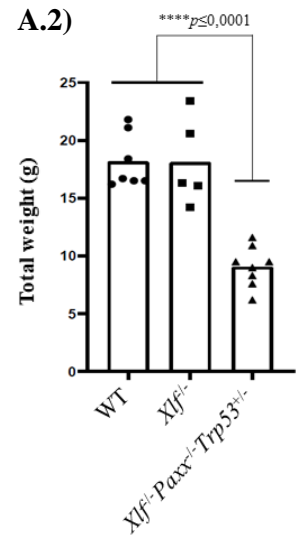
*Xlf<sup>-/-</sup>Paxx<sup>-/-</sup>Trp53<sup>+/-</sup>* mice were significantly lighter than age-matched controls (Figure 12, A). Also, the weights of spleen and thymus were reduced in *Xlf<sup>-/-</sup>Paxx<sup>-/-</sup>Trp53<sup>+/-</sup>* mice (Figures 12, B and C). Similarly, there was a noteworthy lower number of splenocyte, thymocyte and bone marrow cells in *Xlf<sup>-/-</sup>Paxx<sup>-/-</sup>Trp53<sup>+/-</sup>* mice when compared to *Xlf<sup>-/-</sup>* and WT mice (Figure 12, D).

**Figure 12**

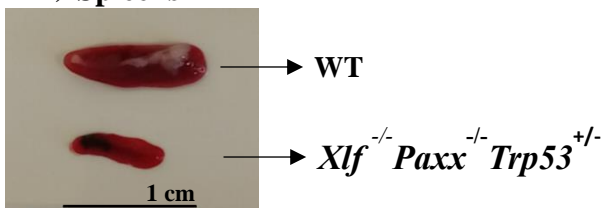
**A.1)**



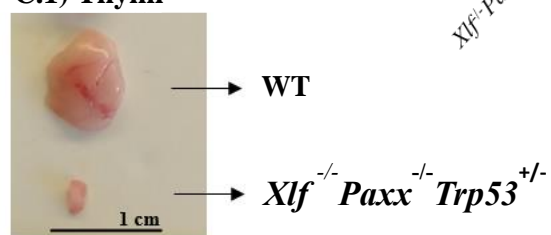
**A.2)**



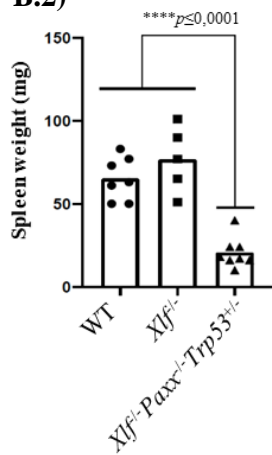
**B.1) Splens**



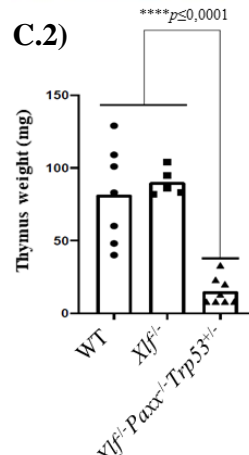
**C.1) Thymi**



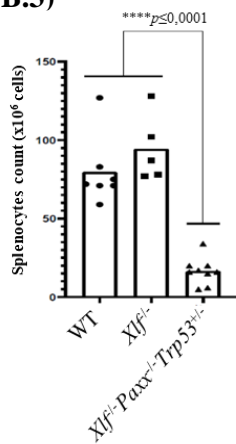
**B.2)**



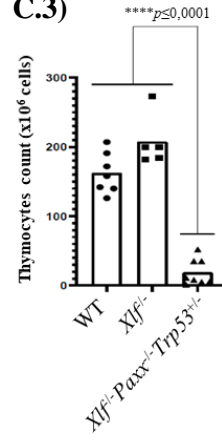
**C.2)**



**B.3)**



**C.3)**



**D)**

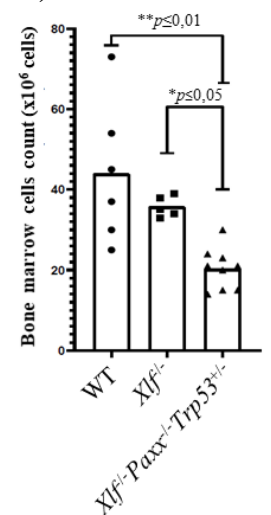


**Figure 12.** B and T cell development in *Xlf<sup>-/-</sup>Paxx<sup>-/-</sup>Trp53<sup>+/-</sup>* mice. **A.1)** Comparison in body size of *Xlf<sup>-/-</sup>Paxx<sup>-/-</sup>Trp53<sup>+/-</sup>* and WT mice. **A.2)** Total body weight (g) of WT, *Xlf<sup>-/-</sup>* and *Xlf<sup>-/-</sup>Paxx<sup>-/-</sup>Trp53<sup>+/-</sup>* mice.

**B.1)** Spleens, isolated from *Xlf<sup>-/-</sup> Paxx<sup>-/-</sup> Trp53<sup>+/-</sup>* and WT mice. **B.2)** Weight (mg) of spleens from WT, *Xlf<sup>-/-</sup>* and *Xlf<sup>-/-</sup> Paxx<sup>-/-</sup> Trp53<sup>+/-</sup>* mice. **B.3)** The number of ( $\times 10^6$ ) splenocytes of WT, *Xlf<sup>-/-</sup>* and *Xlf<sup>-/-</sup> Paxx<sup>-/-</sup> Trp53<sup>+/-</sup>* mice. **C.1)** Thymi, isolated from WT and *Xlf<sup>-/-</sup> Paxx<sup>-/-</sup> Trp53<sup>+/-</sup>* mice. **C.2)** Weight (mg) of thymi from WT, *Xlf<sup>-/-</sup>* and *Xlf<sup>-/-</sup> Paxx<sup>-/-</sup> Trp53<sup>+/-</sup>* mice. **C.3)** The number of ( $\times 10^6$ ) thymocytes of WT, *Xlf<sup>-/-</sup>* and *Xlf<sup>-/-</sup> Paxx<sup>-/-</sup> Trp53<sup>+/-</sup>* mice. **D)** The number ( $\times 10^6$ ) of bone marrow cells of WT, *Xlf<sup>-/-</sup>* and *Xlf<sup>-/-</sup> Paxx<sup>-/-</sup> Trp53<sup>+/-</sup>* mice. Erythrocytes were lysed during the sample preparation and not counted. Not significant n.s.,  $p > 0,005$ ,  $*p \leq 0,05$ ,  $**p \leq 0,01$ ,  $***p \leq 0,001$ ,  $****p \leq 0,0001$ .

### 4.3 B and T cell development in *Xlf<sup>-/-</sup>Paxx<sup>-/-</sup>Trp53<sup>+/-</sup>* mice

Splenocytes, thymocytes and bone marrow cells of *Xlf<sup>-/-</sup>Paxx<sup>-/-</sup>Trp53<sup>+/-</sup>*, *Xlf<sup>-/-</sup>* and WT mice were stained with specific antibodies to examine the proportion and distribution of lymphocytes by flow cytometry analysis.

Splenocytes were marked with anti-CD19 (B cell marker) and anti-CD3 (T cell marker) to portray B and T cell proportion in the spleen of *Xlf<sup>-/-</sup>Paxx<sup>-/-</sup>Trp53<sup>+/-</sup>*, *Xlf<sup>-/-</sup>* and WT mice. Also, splenocytes and thymocytes of the mentioned mice were immunostained with anti-CD4 (T helper cell marker) and anti-CD8 (T cytotoxic cell marker) antibodies to specify T cell subsets frequency in the spleen and thymus. Lastly, anti-CD45R/B220 (B cell marker), anti-CD43 (pro-B cell marker) and anti-IgM (B cells that crossed V(D)J recombination) were applied to demonstrate B cell development in the bone marrow.

There was an extreme reduction in the proportion of splenic B and T lymphocyte of *Xlf<sup>-/-</sup>Paxx<sup>-/-</sup>Trp53<sup>+/-</sup>* mice when compared to *Xlf<sup>-/-</sup>* and WT controls (Figure 13). Similarly, the number of splenic B and T cells of *Xlf<sup>-/-</sup>Paxx<sup>-/-</sup>Trp53<sup>+/-</sup>* mice were considerably reduced in comparison to *Xlf<sup>-/-</sup>* and WT controls (Figure 13).

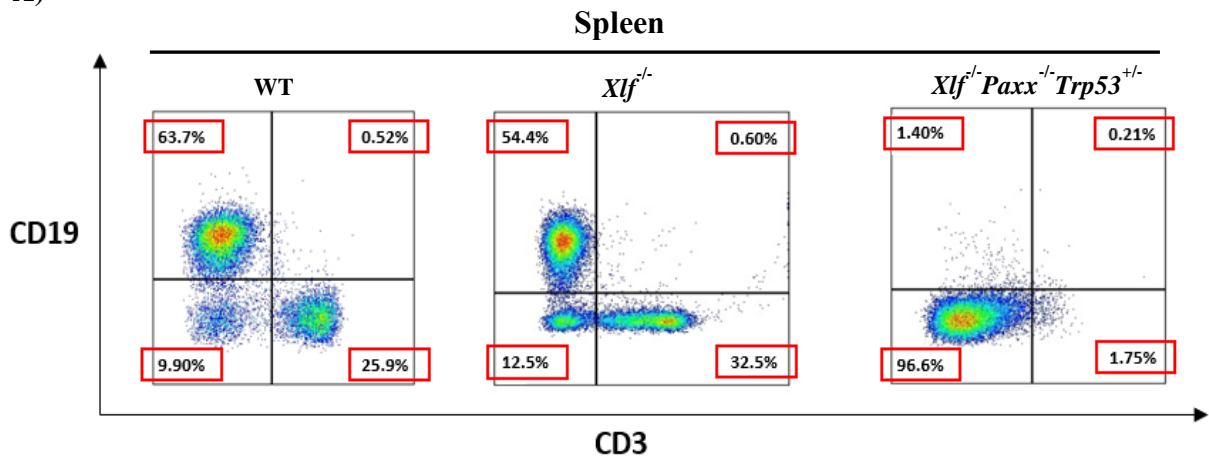
Consonantly, T helper (CD4<sup>+</sup>) and T cytotoxic (CD8<sup>+</sup>) of spleen had a lower percentage and number in *Xlf<sup>-/-</sup>Paxx<sup>-/-</sup>Trp53<sup>+/-</sup>* mice when compared to *Xlf<sup>-/-</sup>* and WT (Figure 14). Likewise, the proportion and number of thymic CD4<sup>+</sup>, CD8<sup>+</sup> and CD4<sup>+</sup>CD8<sup>+</sup> T cells were reduced in *Xlf<sup>-/-</sup>Paxx<sup>-/-</sup>Trp53<sup>+/-</sup>* mice, compared to control mice (Figure 15).

Flow cytometry analysis of B220<sup>+</sup> (B cell), CD43<sup>+</sup> (pro-B cell) and IgM<sup>+</sup> (B cells that crossed V(D)J recombination) cells of bone marrow demonstrated that the proportion of B220<sup>+</sup> cells is not considerably changed, comparing *Xlf<sup>-/-</sup>Paxx<sup>-/-</sup>Trp53<sup>+/-</sup>* mice to the controls. While, the frequency of CD43<sup>+</sup> cells is increased and proportion of IgM<sup>+</sup> cells is decreased in bone marrow of *Xlf<sup>-/-</sup>Paxx<sup>-/-</sup>Trp53<sup>+/-</sup>* mice (Figure 16).

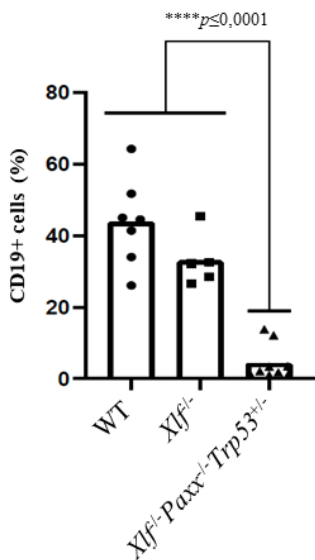
To conclude, B cell development is arrested at pro-B cell stage in bone marrow of *Xlf<sup>-/-</sup>Paxx<sup>-/-</sup>Trp53<sup>+/-</sup>* mice.

**Figure 13**

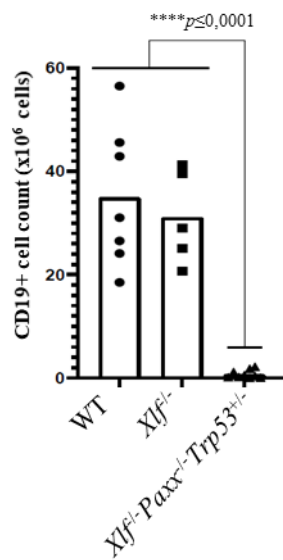
A)



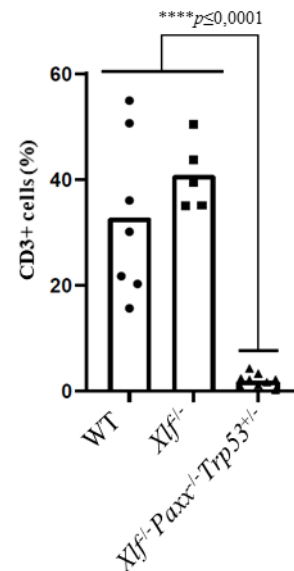
B.1)



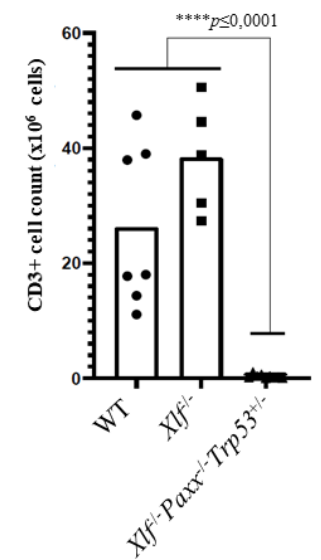
B.2)



C.1)



C.2)



D)

Mice	Cell frequencies (%), Spleen		Number of cells (x10 <sup>6</sup> ), Spleen	
	CD3+	CD19+	CD3+	CD19+
WT	31.23	42.84	27.13	37.29
<i>Xlf</i> <sup>-/-</sup>	42.30	30.47	38.27	32.65
<i>Xlf</i> <sup>-/-</sup> <i>Paxx</i> <sup>-/-</sup> <i>Trp53</i> <sup>+/-</sup>	4.18	1.59	0.20	0.71

**Figure 13.** The frequency of splenic B and T cells in *Xlf*<sup>-/-</sup>*Paxx*<sup>-/-</sup>*Trp53*<sup>+/-</sup> mice. **A)** Portray of flow cytometry analysis of CD19+ (B cell) and CD3+ (T cell) splenocytes, frequencies (%) are indicated. **B.1)** Comparison in splenic CD19+ cells (%) **B.2)** The number (x10<sup>6</sup>) of splenic CD19+ cells **C.1)** Comparison in splenic CD3+ cells (%) **C.2)** The number of (x10<sup>6</sup>) splenic CD3+ cells **D)** The average statistic of splenic B and T lymphocytes of WT, *Xlf*<sup>-/-</sup> and *Xlf*<sup>-/-</sup>*Paxx*<sup>-/-</sup>*Trp53*<sup>+/-</sup> mice. Erythrocytes were lysed during the sample preparation and not counted. Not significant n.s., *p*>0,005, \**p*≤0,05, \*\**p*≤0,01, \*\*\**p*≤0,001, \*\*\*\**p*≤0,0001.

**Figure 14**

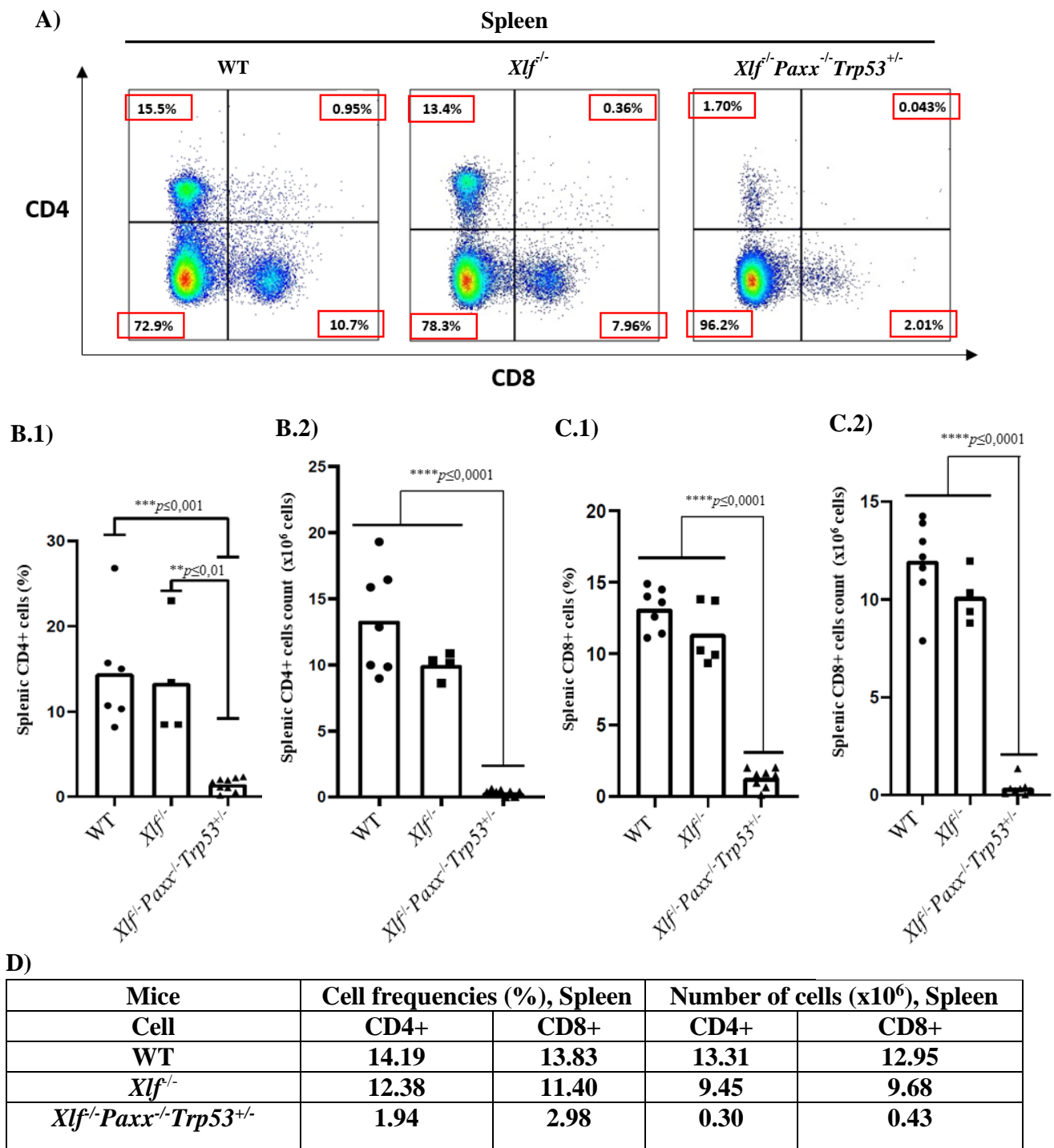
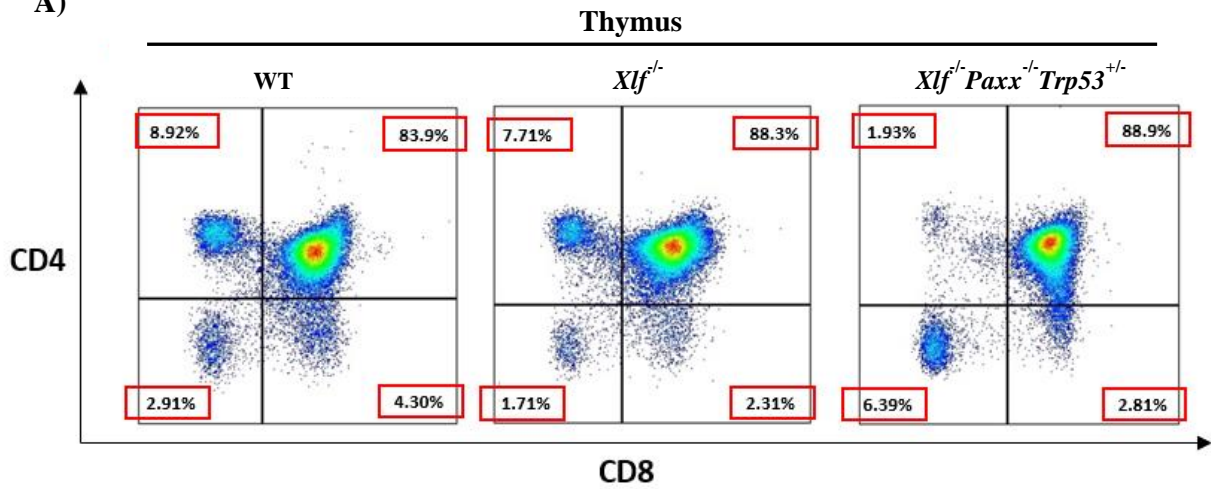


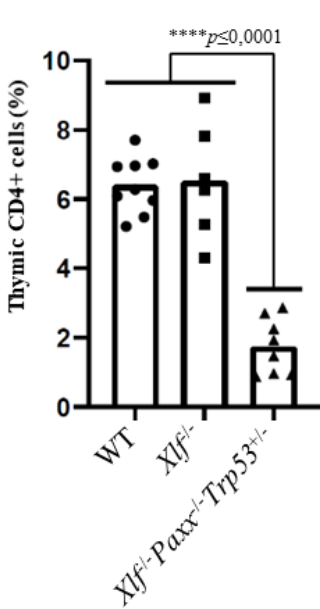
**Figure 14.** The frequency of splenic T cell subsets (CD4<sup>+</sup> and CD8<sup>+</sup>) in *Xlf*<sup>-/-</sup>*Paxx*<sup>-/-</sup>*Trp53*<sup>+/-</sup> mice. **A)** Illustration of flow cytometry analysis of CD8<sup>+</sup> (T cytotoxic) and CD4<sup>+</sup> (T helper) splenocytes, frequencies (%) are indicated. **B.1)** Comparison in splenic CD4<sup>+</sup> cells (%). **B.2)** The number (x10<sup>6</sup>) of splenic CD4<sup>+</sup> cells. **C.1)** Comparison in splenic CD8<sup>+</sup> cells (%). **C.2)** The number (x10<sup>6</sup>) of splenic CD8<sup>+</sup> cells. **D)** The average statistics of splenic T lymphocyte subsets of *Xlf*<sup>-/-</sup>*Paxx*<sup>-/-</sup>*Trp53*<sup>+/-</sup>, *Xlf*<sup>-/-</sup> and WT mice. Erythrocytes were lysed during the sample preparation and not counted. Not significant n.s.,  $p > 0,005$ ,  $*p \leq 0,05$ ,  $**p \leq 0,01$ ,  $***p \leq 0,001$ ,  $****p \leq 0,0001$ .

**Figure 15**

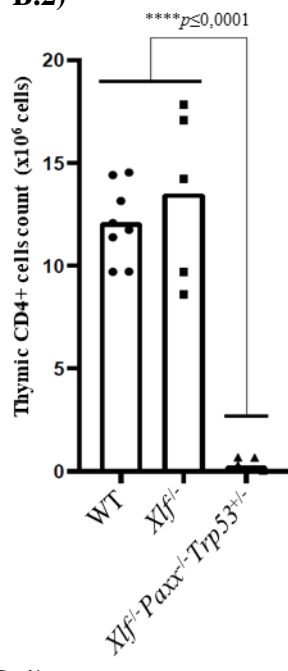
A)



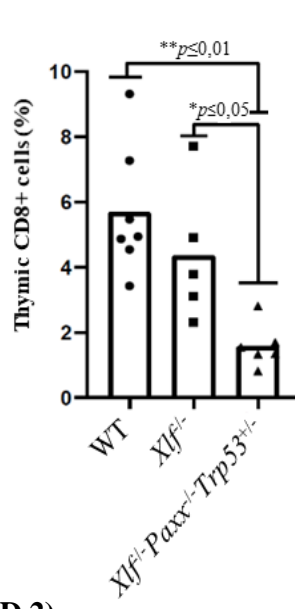
B.1)



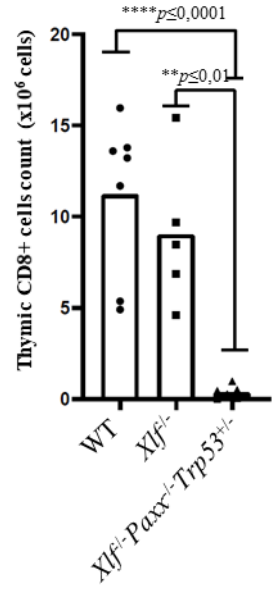
B.2)



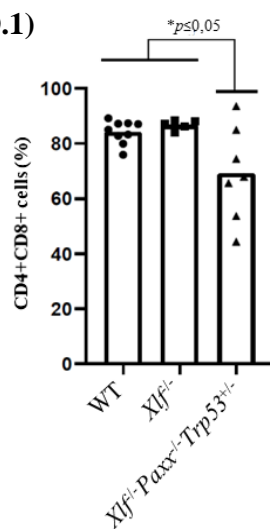
C.1)



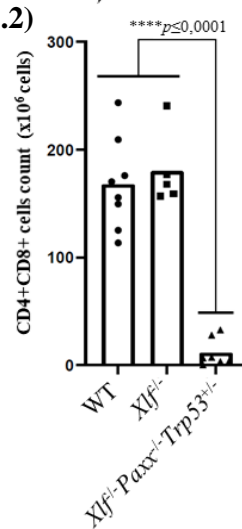
C.2)



D.1)



D.2)



E)

Mice	Cell frequencies (%), Thymus			Number of cells (x10 <sup>6</sup> ), Thymus		
	CD4+	CD8+	CD4+CD8+	CD4+	CD8+	CD4+CD8+
WT	6.53	5.03	85.62	9.67	11.05	163.5
<i>Xlf</i> <sup>-/-</sup>	6.87	4.21	87.33	12.16	7.55	188.2
<i>Xlf</i> <sup>-/-</sup> <i>Paxx</i> <sup>-/-</sup> <i>Trp53</i> <sup>+/-</sup>	1.76	1.63	66.21	0.77	0.73	9.2

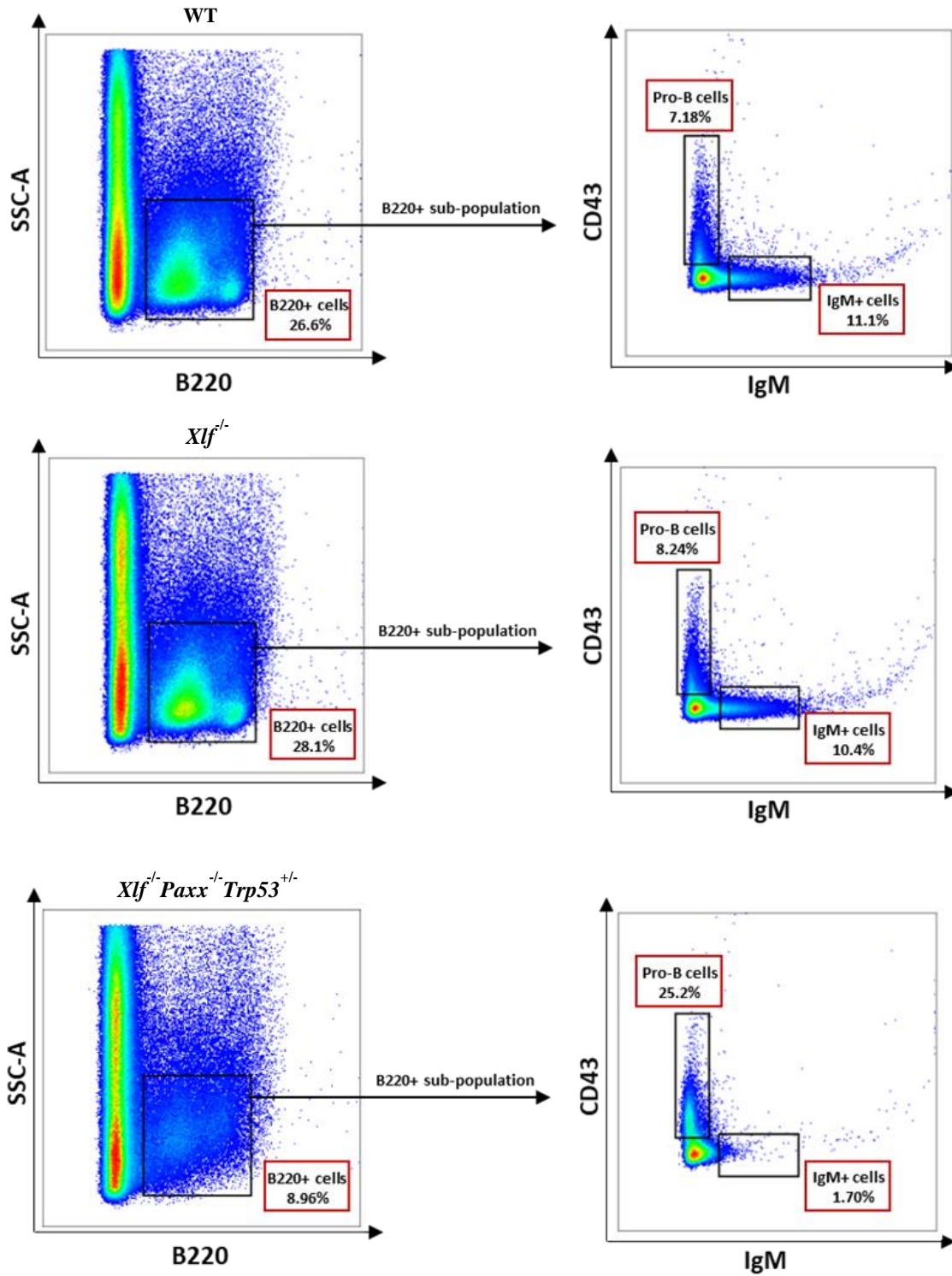
**Figure 15.** The frequency of thymic T cell subsets (CD4+, CD8+ and CD4+CD8+) in *Xlf*<sup>-/-</sup>*Paxx*<sup>-/-</sup>*Trp53*<sup>+/-</sup> mice. **A)** Example of flow cytometry analysis of CD8+ (T cytotoxic), CD4+ (T helper) and CD4+CD8+ (double-positive T cell) thymocytes, frequencies (%) are indicated. **B.1)** Comparison in thymic CD4+ cells (%) **B.2)** The number (x10<sup>6</sup>) of thymic CD4+ cells **C.1)** Comparison in thymic CD8+ cells (%) **C.2)** The number (x10<sup>6</sup>) of thymic CD8+ cells **D.1)** Comparison in CD4+CD8+ cells (%) **D.2)** The number (x10<sup>6</sup>) of CD4+CD8+ cells **E)** The average statistics of thymic T lymphocyte subsets of *Xlf*<sup>-/-</sup>*Paxx*<sup>-/-</sup>*Trp53*<sup>+/-</sup>, *Xlf*<sup>-/-</sup> and WT mice. Erythrocytes were lysed during the sample preparation and not counted. Not significant n.s.,  $p > 0,005$ , \* $p \leq 0,05$ , \*\* $p \leq 0,01$ , \*\*\* $p \leq 0,001$ , \*\*\*\* $p \leq 0,0001$ .

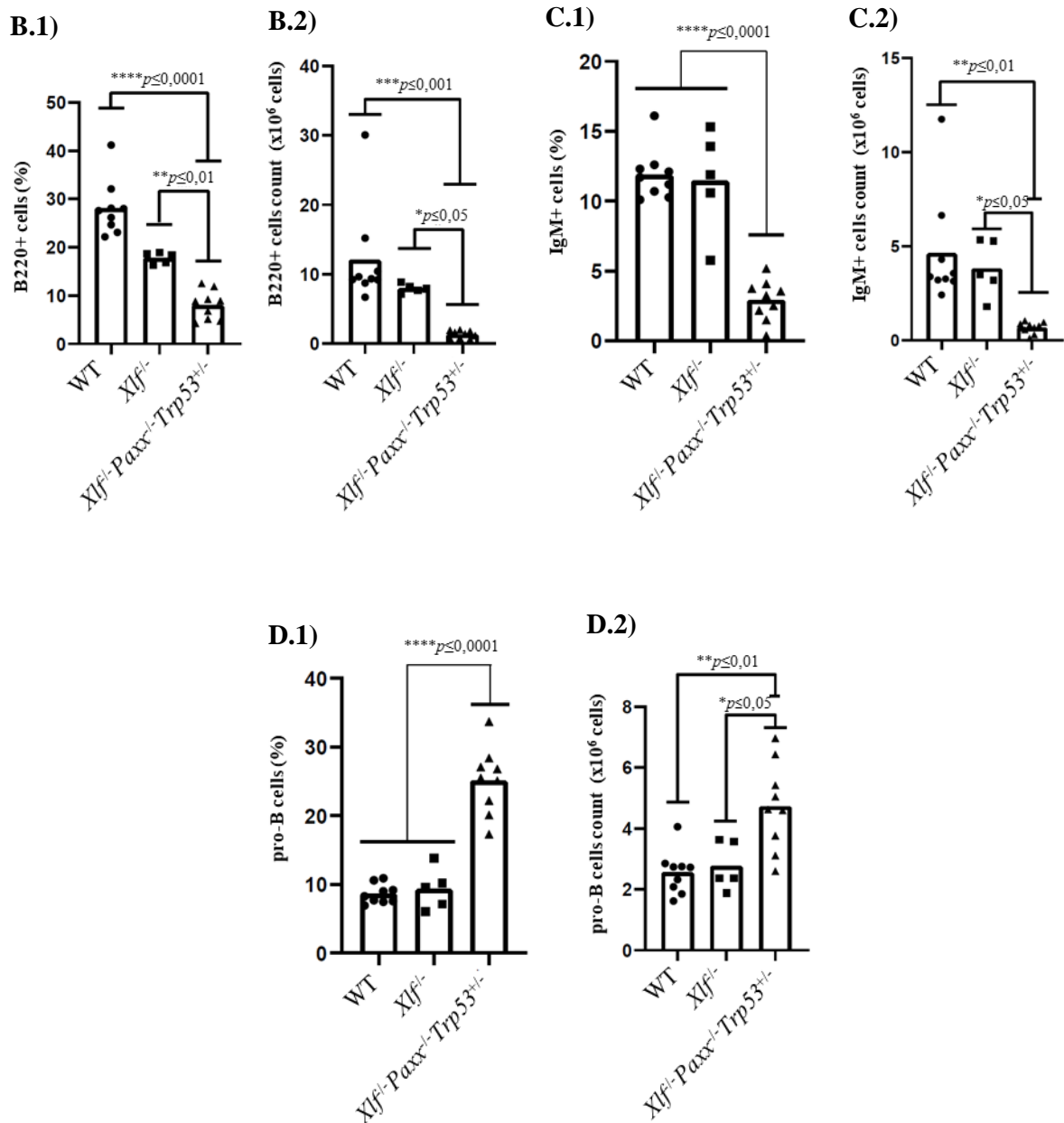


Figure 16

A)

Bone marrow





E)

Mice	Cell frequencies (%), Bone marrow			Number of cells (x10 <sup>6</sup> ), Bone marrow		
	B220+	CD43+	IgM+	B220+	CD43+	IgM+
WT	25.81	7.49	11.59	10.49	2.98	4.67
<i>Xlf</i> <sup>-/-</sup>	20.21	9.17	10.74	7.96	3.89	3.47
<i>Xlf</i> <sup>-/-</sup> <i>Paxx</i> <sup>-/-</sup> <i>Trp53</i> <sup>+/-</sup>	9.19	25.27	3.08	1.93	4.97	0.63

**Figure 16.** The frequency of B220+, pro-B and IgM+ cells in the bone marrow of *Xlf*<sup>-/-</sup>*Paxx*<sup>-/-</sup>*Trp53*<sup>+/-</sup> mice. A) Demonstration of flow cytometry analysis of WT, *Xlf*<sup>-/-</sup> and *Xlf*<sup>-/-</sup>*Paxx*<sup>-/-</sup>*Trp53*<sup>+/-</sup> mice. Bone marrow cells were distinguished by anti-B220, anti-CD43 and anti-IgM antibodies. Figures at the left side show the proportion of B220+ cells (B cells) in bone marrow of WT, *Xlf*<sup>-/-</sup> and *Xlf*<sup>-/-</sup>*Paxx*<sup>-/-</sup>*Trp53*<sup>+/-</sup> mice. Figures at the right side represent the sub-population of B220+ cells including pro-B (CD43+IgM-

) and IgM+ (CD43-IgM+) cells for the mentioned genotypes. Distribution frequencies (%) are indicated. **B.1)** Proportion B220+ cells in bone marrow (%). **B.2)** The number ( $\times 10^6$ ) of B220+ cells in bone marrow. **C.1)** Proportion of IgM+ cells in bone marrow (%). **C.2)** The number ( $\times 10^6$ ) of IgM+ cells in bone marrow. **D.1)** Proportion of pro-B cells in bone marrow (%). **D.2)** The number ( $\times 10^6$ ) of pro-B cells in bone marrow. **E)** Average statistics of B220+, CD43+ and IgM+ cells in bone marrow of WT, *Xlf*<sup>-/-</sup> and *Xlf*<sup>-/-</sup>*Paxx*<sup>-/-</sup>*Trp53*<sup>+/-</sup> mice. Erythrocytes were lysed during the sample preparation and not counted. Not significant n.s.,  $p > 0,005$ ,  $*p \leq 0,05$ ,  $**p \leq 0,01$ ,  $***p \leq 0,001$ ,  $****p \leq 0,0001$ .

#### 4.4 Genetic interaction between *Mri* and *Dna-pkcs* genes in mice

In order to perform my third research aim, I genotyped 66 mice in total. All the examined mice were from *Mri*<sup>+/-</sup>*Dna-pkcs*<sup>+/-</sup> parents. Mendelian distribution of expected and the number of obtained offspring are mentioned in Table 4. According to the mendelian distribution I should have found 4 *Mri*<sup>-/-</sup>*Dna-pkcs*<sup>-/-</sup> mice. Noticeably, no *Mri*<sup>-/-</sup>*Dna-pkcs*<sup>-/-</sup> mice were observed. It may suggest that combined inactivation of *Mri* and *Dna-pkcs* genes leads to embryonic lethality. While 5 *Mri*<sup>+/-</sup>*Dna-pkcs*<sup>-/-</sup> mice were detected, no DNA-PKcs-deficient mice were identified, suggesting that the number of mice analyzed may be too low to make a solid conclusion, and total 100-400 mice need to be analyzed in the future.

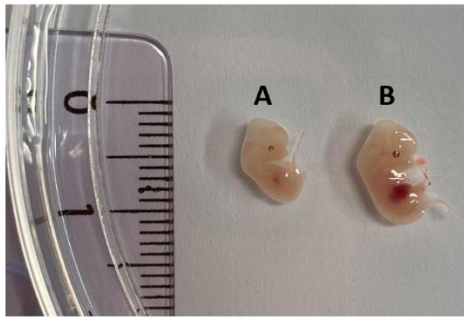
Genotype	Number of offspring, P30	Expected 1:2:1:2:4:2:1:2:1
<i>Mri</i> <sup>+/+</sup> <i>Dna-pkcs</i> <sup>+/+</sup>	5	4.12
<i>Mri</i> <sup>+/+</sup> <i>Dna-pkcs</i> <sup>+/-</sup>	4	8.24
<i>Mri</i> <sup>+/+</sup> <i>Dna-pkcs</i> <sup>-/-</sup>	0	4.12
<i>Mri</i> <sup>+/-</sup> <i>Dna-pkcs</i> <sup>+/+</sup>	9	8.24
<i>Mri</i> <sup>+/-</sup> <i>Dna-pkcs</i> <sup>+/-</sup>	19	16.48
<i>Mri</i> <sup>+/-</sup> <i>Dna-pkcs</i> <sup>-/-</sup>	5	8.24
<i>Mri</i> <sup>-/-</sup> <i>Dna-pkcs</i> <sup>+/+</sup>	12	4.12
<i>Mri</i> <sup>-/-</sup> <i>Dna-pkcs</i> <sup>+/-</sup>	12	8.24
<i>Mri</i> <sup>-/-</sup> <i>Dna-pkcs</i> <sup>-/-</sup>	0	4.12
<b>Total</b>	<b>66</b>	<b>66</b>

**Table 4.** The number of thirty-day-old mice (P30) of the indicated genotypes. Mendelian distribution is provided in the third column. Both parents were *Mri*<sup>+/-</sup>*Dna-pkcs*<sup>+/-</sup>. In total, 66 mice were analyzed.

Although, my co-supervisor Sergio Castaneda and I planned to assess the phenotype of *Mri.Dnapkcs* embryos. We examined embryos at embryonic day E14.5, isolated from *Mri*<sup>+/-</sup>*Dna-pkcs*<sup>+/-</sup> female (both parents were *Mri*<sup>+/-</sup>*Dna-pkcs*<sup>+/-</sup>). Noticeably, two embryos were smaller and lighter in comparison to the others (Figure 17). Genotyping PCR confirmed that the smaller embryos were *Mri*<sup>-/-</sup>*Dna-pkcs*<sup>-/-</sup>.

**Figure 17**

A)



B)

Embryos	Genotype	Weight (g)
1	<i>Mri<sup>-/-</sup>Dna-pkcs<sup>-/-</sup></i>	0.0630
2	<i>Mri<sup>-/-</sup>Dna-pkcs<sup>-/-</sup></i>	0.0633
3	<i>Mri<sup>-/-</sup>Dna-pkcs<sup>+/-</sup></i>	0.1082
4	<i>Mri<sup>-/-</sup>Dna-pkcs<sup>+/-</sup></i>	0.1010

**Figure 17.** Comparison of *Mri<sup>-/-</sup>Dna-pkcs<sup>-/-</sup>* double knock out with *Mri<sup>-/-</sup>Dna-pkcs<sup>+/-</sup>* embryos. **A)** As can be observed, the size of *Mri<sup>-/-</sup>Dna-pkcs<sup>-/-</sup>* deficient embryo is smaller than *Mri<sup>-/-</sup>Dna-pkcs<sup>+/-</sup>* embryo. **B)** Two *Mri<sup>-/-</sup>Dna-pkcs<sup>-/-</sup>* embryos and two *Mri<sup>-/-</sup>Dna-pkcs<sup>+/-</sup>* embryos were weighted. Embryos lacking Mri and DNA-PKcs had lower weight (g) when compared to *Mri<sup>-/-</sup>Dna-pkcs<sup>+/-</sup>* embryos.

#### 4.5 No genetic interaction between *Mri* and *Paxx* genes in mice

To perform my fourth research aim, I genotyped 60 mice in total. The distribution of the expected and analyzed mice is indicated in Table 5. All the analyzed mice were generated from *Mri*<sup>+/-</sup>*Paxx*<sup>+/-</sup> parents.

Genotype	Number of offspring, P30	Expected 1:2:1:2:4:2:1:2:1
<i>Mri</i> <sup>+/+</sup> <i>Paxx</i> <sup>+/+</sup>	8	3.75
<i>Mri</i> <sup>+/+</sup> <i>Paxx</i> <sup>+/-</sup>	8	7.5
<i>Mri</i> <sup>+/+</sup> <i>Paxx</i> <sup>-/-</sup>	2	3.75
<i>Mri</i> <sup>+/-</sup> <i>Paxx</i> <sup>+/+</sup>	17	7.5
<i>Mri</i> <sup>+/-</sup> <i>Paxx</i> <sup>+/-</sup>	6	15
<i>Mri</i> <sup>+/-</sup> <i>Paxx</i> <sup>-/-</sup>	4	7.5
<i>Mri</i> <sup>-/-</sup> <i>Paxx</i> <sup>+/+</sup>	7	3.75
<i>Mri</i> <sup>-/-</sup> <i>Paxx</i> <sup>+/-</sup>	1	7.5
<i>Mri</i> <sup>-/-</sup> <i>Paxx</i> <sup>-/-</sup>	7	3.75
<b>Total</b>	<b>60</b>	<b>60</b>

**Table 5.** The first column indicates the genotypes. The number of thirty-day-old mice (P30) is mentioned in the second column. The third column provides the mendelian distribution. Both parents had *Mri*<sup>+/-</sup>*Paxx*<sup>+/-</sup> genotype.

To elucidate the genetic interaction between the NHEJ accessory factors *Mri* and *Paxx* in mice, I examined 16 mice, including five *Mri*<sup>-/-</sup> *Paxx*<sup>-/-</sup>, four *Mri*<sup>-/-</sup> and seven WT mice. *Mri*<sup>-/-</sup> mice were used as single knock out control. The *Paxx*<sup>-/-</sup> mice were not available at the time of experiments. However, lack of PAXX does not affect the lymphocyte development in mice [9, 34-36, 44, 51]. To investigate the phenotypic impact of *Mri*<sup>-/-</sup>*Paxx*<sup>-/-</sup> double deficiency on immune system development in mice, the weights of the whole body, spleen and thymus were measured. Furthermore, the number of splenocytes, thymocytes and bone marrow cells was recorded.

There was no significant difference between controls and *Mri*<sup>-/-</sup>*Paxx*<sup>-/-</sup> mice in the body weight (Figure 18, A). Moreover, there were no notable changes in the spleen weight and the number of splenocytes between WT, *Mri*<sup>-/-</sup> and *Mri*<sup>-/-</sup> *Paxx*<sup>-/-</sup> mice (Figure 18, B). Likewise, no consequential variations were detected in the thymus weight and the number of thymocytes of *Mri*<sup>-/-</sup>*Paxx*<sup>-/-</sup> mice when compared to *Mri*<sup>-/-</sup> and WT controls (Figure 18, C). The number of bone marrow cells of WT, *Mri*<sup>-/-</sup> and *Mri*<sup>-/-</sup>*Paxx*<sup>-/-</sup> mice was similar as well (Figure 18, D).

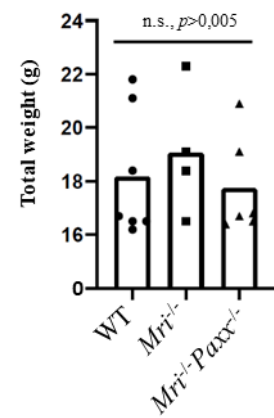
Therefore, the mentioned results suggest that there is no genetic interaction between *Mri* and *Paxx* genes in mice.

**Figure 18**

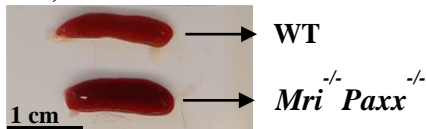
**A.1)**



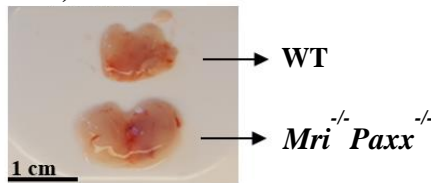
**A.2)**



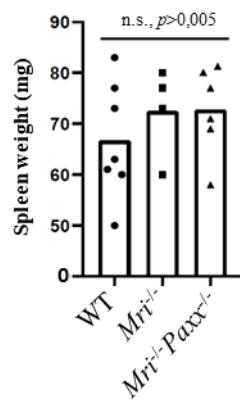
**B.1) Splens**



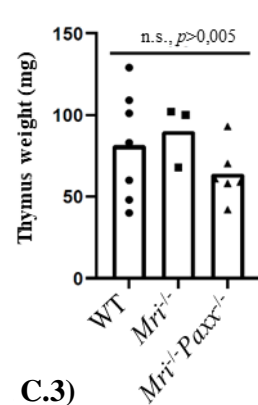
**C.1) Thymi**



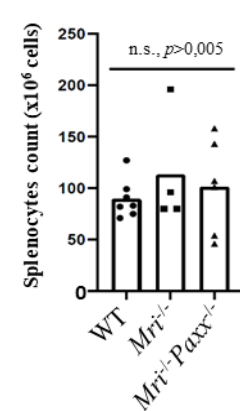
**B.2)**



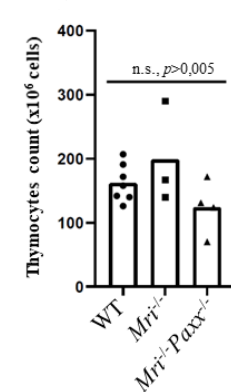
**C.2)**



**B.3)**



**C.3)**



**D)**

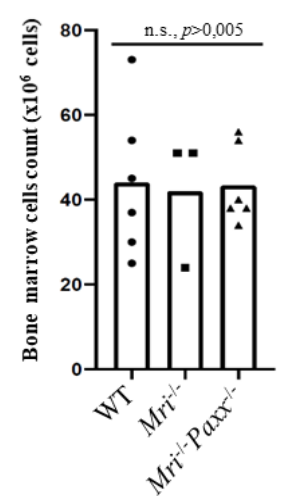


**Figure 18.** Immune system development in *Mri*<sup>-/-</sup>*Paxx*<sup>-/-</sup> mice. **A.1)** Comparison of *Mri*<sup>-/-</sup>*Paxx*<sup>-/-</sup> and WT mice in body size. **B.1)** Splens, isolated from WT and *Mri*<sup>-/-</sup>*Paxx*<sup>-/-</sup> mice. **B.2)** Weight (mg) of splens from WT, *Mri*<sup>+/-</sup> and *Mri*<sup>-/-</sup>*Paxx*<sup>-/-</sup> mice. **B.3)** The number of (x10<sup>6</sup>) splenocytes of WT, *Mri*<sup>+/-</sup> and *Mri*<sup>-/-</sup>*Paxx*<sup>-/-</sup> mice. **C.1)** Thymi, isolated from WT and *Mri*<sup>-/-</sup>*Paxx*<sup>-/-</sup> mice. **C.2)** Weight (mg) of thymi from WT, *Mri*<sup>+/-</sup> and *Mri*<sup>-/-</sup>*Paxx*<sup>-/-</sup> mice. **C.3)** The number of (x10<sup>6</sup>) thymocytes of WT, *Mri*<sup>+/-</sup> and *Mri*<sup>-/-</sup>*Paxx*<sup>-/-</sup> mice. **D)** The number (x10<sup>6</sup>) of bone marrow cells from WT, *Mri*<sup>+/-</sup> and *Mri*<sup>-/-</sup>*Paxx*<sup>-/-</sup> mice. Erythrocytes



were lysed during the sample preparation and not counted. Not significant n.s.,  $p > 0,005$ ,  $*p \leq 0,05$ ,  $**p \leq 0,01$ ,  $***p \leq 0,001$ ,  $****p \leq 0,0001$ .

#### **4.6 Proportions of B and T lymphocytes in spleens, thymi and bone marrow of *Mri*<sup>-/-</sup> *Paxx*<sup>-/-</sup> mice**

To examine the impact of *Mri*<sup>-/-</sup>*Paxx*<sup>-/-</sup> double deficiency on B and T cell development in mice, splenocytes, thymocytes and bone marrow cells were isolated from WT (n=7), *Mri*<sup>-/-</sup> (n=4) and *Mri*<sup>-/-</sup>*Paxx*<sup>-/-</sup> (n=5) mice. *Mri*-deficient mice were used as control. The *Paxx*<sup>-/-</sup> control was not available at the time of the experiments. However, PAXX-deficient mice possess normal B and T cell development [9, 34-36, 44, 51]. Hence, isolated cells were immunostained and analyzed by flow cytometry experiment. All analyzed mice were 5 to 8 weeks old.

To determine the proportion of B and T cells in the spleen, anti-CD19 (B cell marker) and anti-CD3 (T cell marker) were used to stain splenocytes. Furthermore, splenocytes and thymocytes were stained with anti-CD4 (T helper marker) and anti-CD8 (T cytotoxic marker) to portray T cell subsets in spleen and thymus. Finally, bone marrow cells were stained with anti-CD45R/B220 (B cell marker), anti-CD43 (pro-B cell marker) and anti-IgM (the marker of B cells that completed V(D)J recombination) to characterize the proportion of B cells in different stages of development in the bone marrow.

The result of B and T cell examination in the spleen is presented in Figure 19. No significant differences between *Mri*<sup>-/-</sup>*Paxx*<sup>-/-</sup> knock out mice were observed when compared to control mice. The proportion of splenic T cell subsets (T helper and T cytotoxic) was similar among *Mri*<sup>-/-</sup>*Paxx*<sup>-/-</sup> mice and controls (Figure 20). Thymic T cell subsets were similar between WT, *Mri*<sup>-/-</sup> and *Mri*<sup>-/-</sup>*Paxx*<sup>-/-</sup> double knock out mice (Figure 21).

Observation of B cell proportion in different stages of development in the bone marrow is displayed in Figure 22. The percentage of B220+ cells (B cell marker), pro-B cells (CD43+IgM-), and IgM+ cells (CD43-IgM+) were similar between examined controls and *Mri*<sup>-/-</sup>*Paxx*<sup>-/-</sup> knock out mice. The reported outcomes reveal that there is no difference in lymphocyte development, comparing *Mri*<sup>-/-</sup>*Paxx*<sup>-/-</sup> double knock out mice to *Mri*<sup>-/-</sup> and WT controls. To sum up, there is no genetic interaction between *Mri* and *Paxx*. *Mri*<sup>-/-</sup>*Paxx*<sup>-/-</sup> mice do not have any deficits in B and T cell development.

**Figure 19**

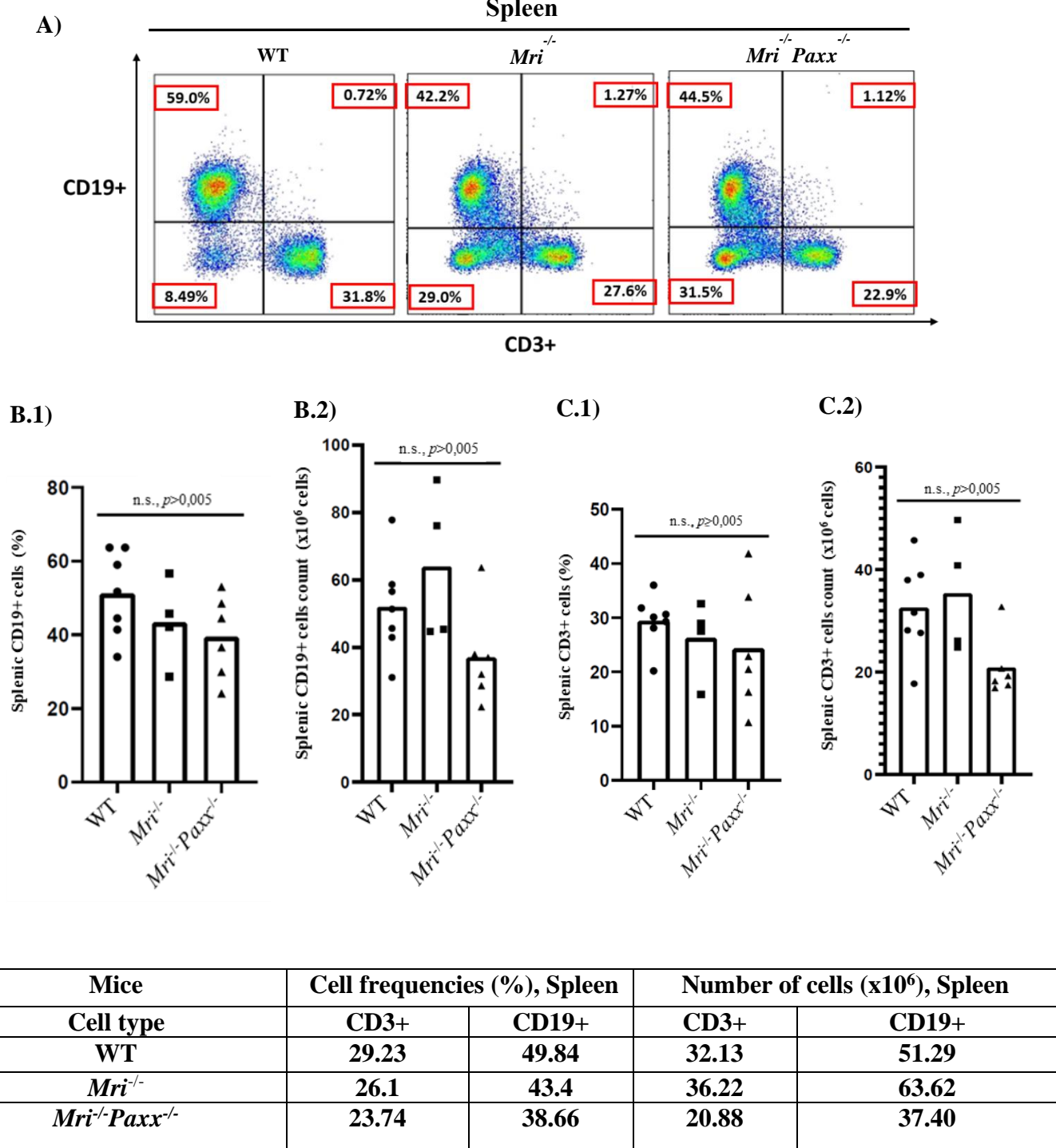
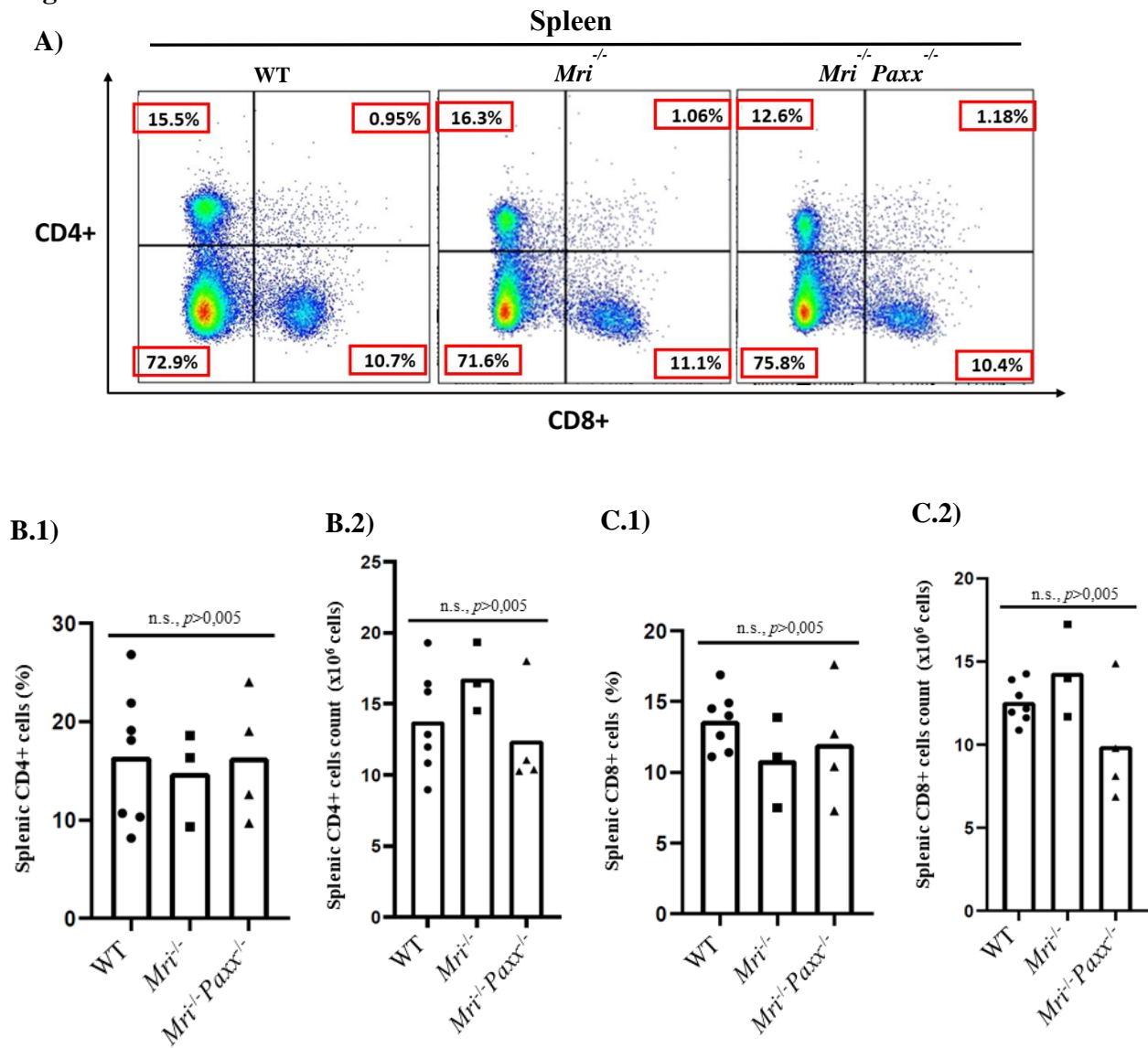


**Figure 19.** Splenic B and T cell frequencies in *Mri*<sup>-/-</sup>*Paxx*<sup>-/-</sup> mice. **A)** Flow cytometry analysis of WT, *Mri*<sup>-/-</sup> and *Mri*<sup>-/-</sup>*Paxx*<sup>-/-</sup> mice. Splenocytes were distinguished by anti-CD3 (T cell marker) and anti-CD19 (B cell marker) markers. Distribution frequencies (%) are demonstrated. **B.1)** Comparison in splenic CD19+ cells (%) **B.2)** The number (x10<sup>6</sup>) of CD19+ cells **C.1)** Comparison in CD3+ cells (%) **C.2)** The number (x10<sup>6</sup>) of CD3+ cells **D)** Average number (x10<sup>6</sup>) and frequencies (%) of splenic B and T cell in *Mri*<sup>-/-</sup>*Paxx*<sup>-/-</sup> and control mice. Erythrocytes were lysed during the sample preparation and not counted. Not significant n.s.,  $p > 0,005$ ,  $*p \leq 0,05$ ,  $**p \leq 0,01$ ,  $***p \leq 0,001$ ,  $****p \leq 0,0001$ .

**Figure 20**

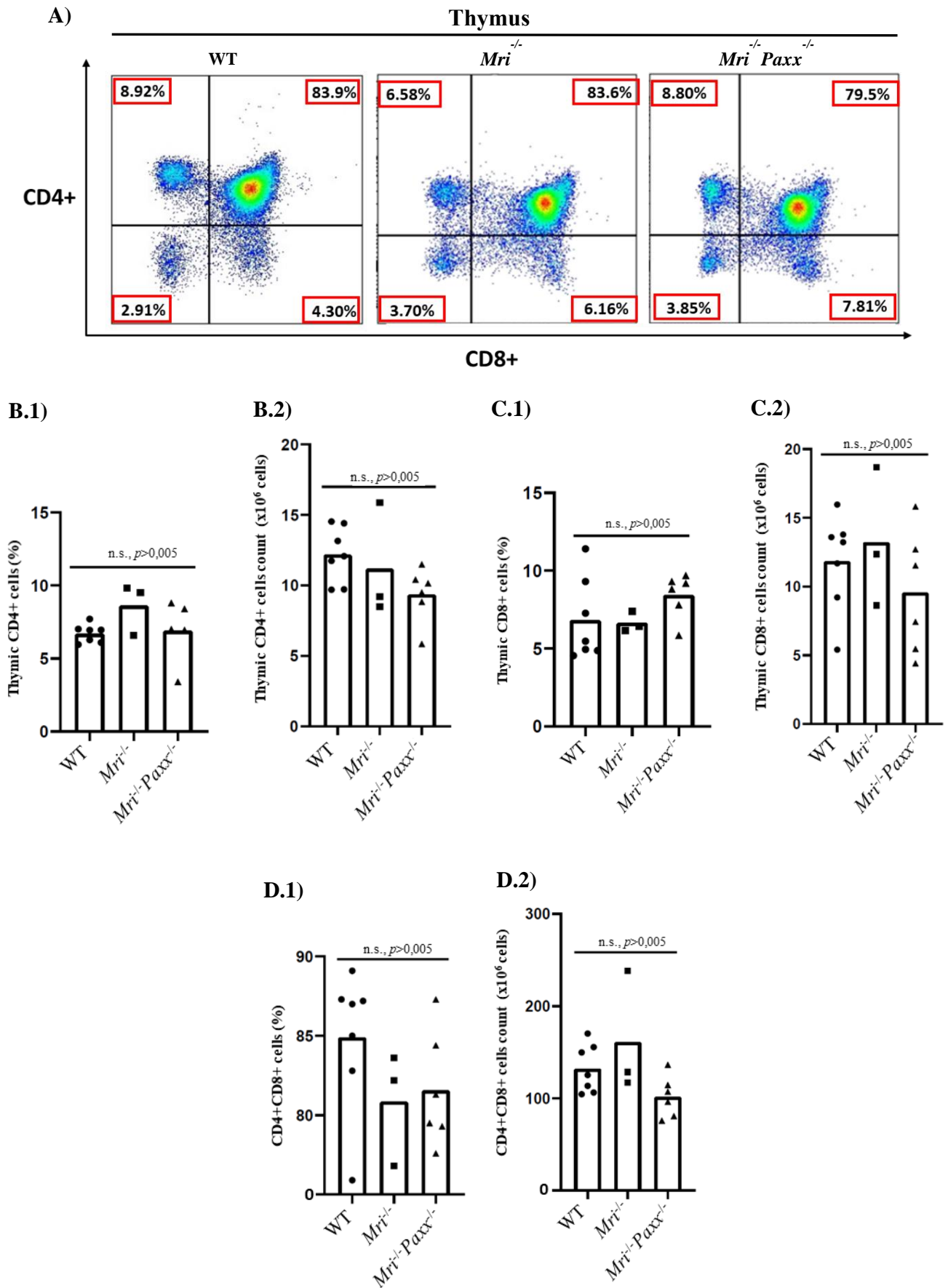


**D)**

Mice	Cell frequencies (%), Spleen		Number of cells (x10 <sup>6</sup> ), Spleen	
	CD4+	CD8+	CD4+	CD8+
WT	16.29	13.83	14.31	12.95
<i>Mri</i> <sup>-/-</sup>	14.80	11.3	16.93	14.48
<i>Mri</i> <sup>-/-</sup> <i>Paxx</i> <sup>-/-</sup>	16.4	12.83	13.19	9.32

**Figure 20.** Splenic CD4<sup>+</sup> (T helper) and CD8<sup>+</sup> (T cytotoxic) cell frequencies in *Mri*<sup>-/-</sup>*Paxx*<sup>-/-</sup> mice  
**A)** Flow cytometry analysis of WT, *Mri*<sup>-/-</sup> and *Mri*<sup>-/-</sup>*Paxx*<sup>-/-</sup> mice. Splenocytes were immunostained by anti-CD4 and anti-CD8 markers. Distribution frequencies (%) are demonstrated. **B.1)** Comparison in splenic CD4+ (%) **B.2)** The number (x10<sup>6</sup>) of splenic CD4+ cells **C.1)** Comparison in splenic CD8+ cells (%) **C.2)** The number (x10<sup>6</sup>) of splenic CD8+ cells **D)** Average statistics of splenic CD4+ and CD8+ cells in *Mri*<sup>-/-</sup>*Paxx*<sup>-/-</sup> and control mice. Erythrocytes were lysed during the sample preparation and not counted. Not significant n.s.,  $p > 0,005$ ,  $*p \leq 0,05$ ,  $**p \leq 0,01$ ,  $***p \leq 0,001$ ,  $****p \leq 0,0001$ .

**Figure 21**

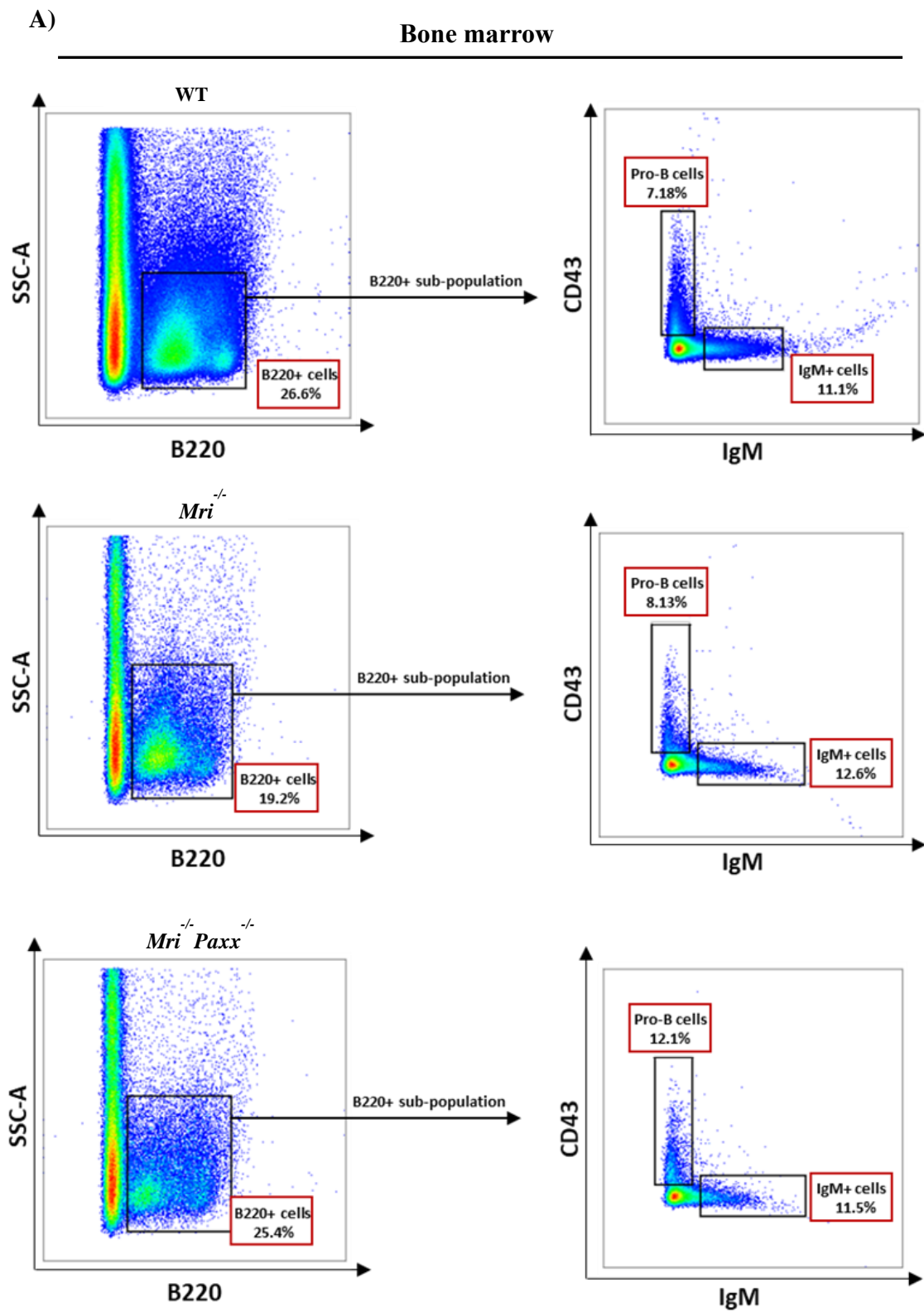


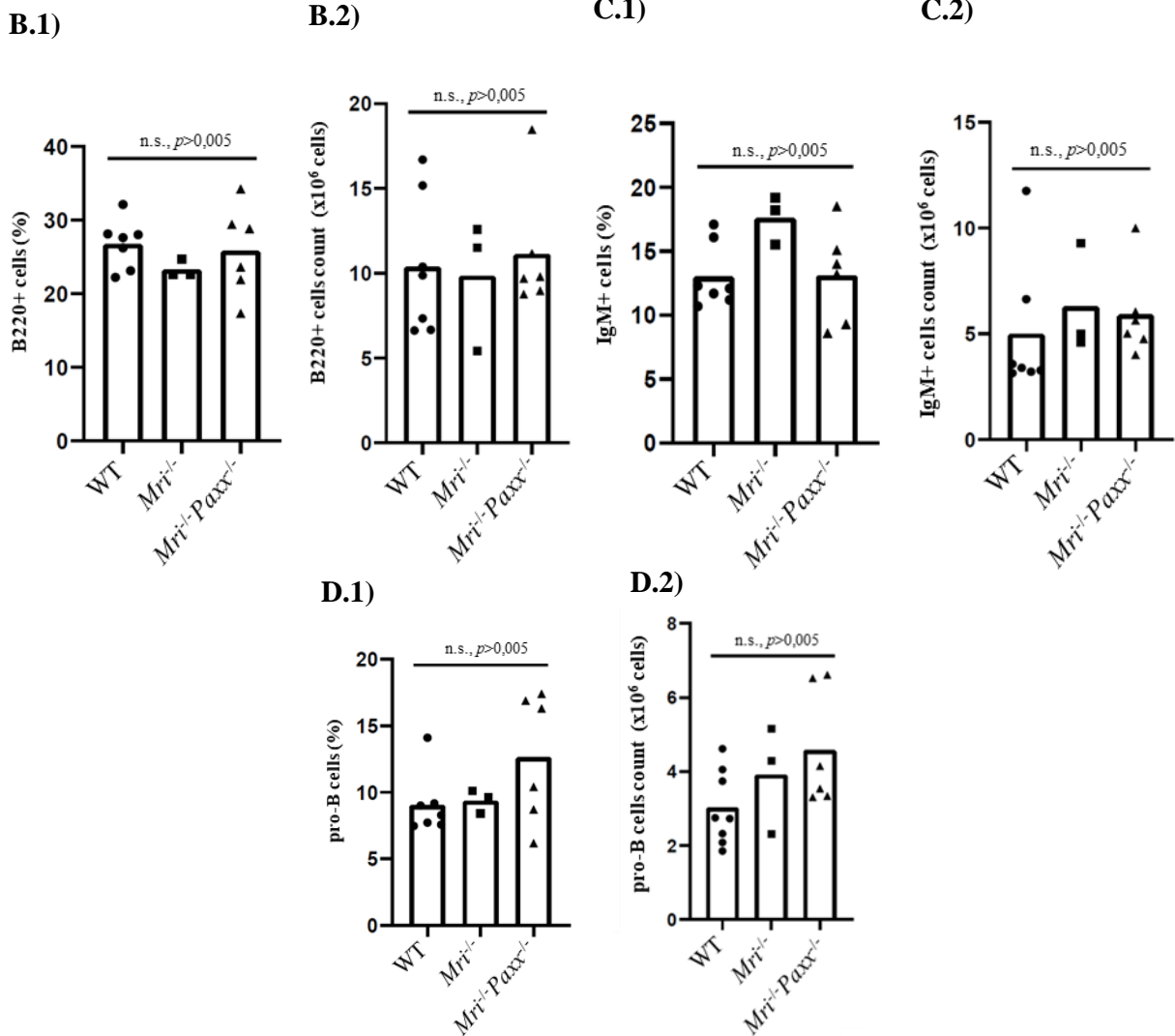
E)

Mice	Cell frequencies (%), Thymus			Number of cells (x10 <sup>6</sup> ), thymus		
Cell type	CD4+	CD8+	CD4+CD8+	CD4+	CD8+	CD4+CD8+
WT	7.24	7.03	84.7	9.67	6.55	127.3
<i>Mri</i> <sup>-/-</sup>	8.04	6.78	81.98	12.54	10.49	162.23
<i>Mri</i> <sup>-/-</sup> <i>Paxx</i> <sup>-/-</sup>	7.67	8.86	83.11	5.76	11.38	93.67

**Figure 21.** The proportion of thymic CD4+ (T helper), CD8+ (T cytotoxic) and CD4+CD8+ (double-positive T cell) in *Mri*<sup>-/-</sup>*Paxx*<sup>-/-</sup> mice. **A)** Portray of flow cytometry analysis of *Mri*<sup>-/-</sup>*Paxx*<sup>-/-</sup> and control mice. Isolated thymocytes were examined by anti-CD4 and anti-CD8 markers. Distribution frequencies (%) are demonstrated. **B.1)** Comparison in thymic CD4+ cells (%) **B.2)** The number (x10<sup>6</sup>) of thymic CD4+ cells **C.1)** Comparison in thymic CD8+ cells (%) **C.2)** The number (x10<sup>6</sup>) of thymic CD8+ cells **D.1)** Comparison in CD4+CD8+cells (%) **D.2)** The number (x10<sup>6</sup>) of CD4+CD8+ cells **E)** Average statistics of thymic CD4+, CD8+ and CD4+CD8+ cells in WT, *Mri*<sup>-/-</sup> and *Mri*<sup>-/-</sup>*Paxx*<sup>-/-</sup> mice. Erythrocytes were lysed during the sample preparation and not counted. Not significant n.s.,  $p > 0,005$ ,  $*p \leq 0,05$ ,  $**p \leq 0,01$ ,  $***p \leq 0,001$ ,  $****p \leq 0,0001$ .

Figure 22





E)

Mice	Cell frequencies (%), Bone marrow			Number of cells (x10 <sup>6</sup> ), Bone marrow		
Cell type	B220+	CD43+	IgM+	B220+	CD43+	IgM+
WT	26.81	9.17	12.95	10.49	2.89	4.67
<i>Mri</i> <sup>-/-</sup>	22.12	9.45	16.85	9.06	3.72	6.69
<i>Mri</i> <sup>-/-</sup> <i>Paxx</i> <sup>-/-</sup>	25.65	13.04	13.18	12.07	4.69	5.66

**Figure 22.** Frequency of B220+, pro-B and IgM+ cells in the bone marrow of *Mri*<sup>-/-</sup>*Paxx*<sup>-/-</sup> mice **A)** Example of flow cytometry analysis of B220+, pro-B and IgM+ cells in the bone marrow of *Mri*<sup>-/-</sup>*Paxx*<sup>-/-</sup>, *Mri*<sup>-/-</sup> and WT mice. The bone marrow cells were distinguished, utilizing anti-B220, anti-CD43 and anti-IgM markers. Figures at the left side show the proportion of B220+ cells (B cells) of the bone marrow of WT, *Mri*<sup>-/-</sup> and *Mri*<sup>-/-</sup>*Paxx*<sup>-/-</sup> mice. Figures at the right side represent the sub-population of B220+ cells including pro-B (CD43+IgM-) and IgM+ cells (CD43-IgM+) for the mentioned mice. Distribution frequencies (%) are demonstrated. **B.1)** Comparison in B220+ cells in bone marrow (%). **B.2)** The number (x10<sup>6</sup>) of B220+ cells in bone marrow. **C.1)** Comparison in IgM+ cells in bone marrow (%). **C.2)** The number (x10<sup>6</sup>) of IgM+ cells in bone marrow. **D.1)** Comparison in pro-B cells (%). **D.2)** The number (x10<sup>6</sup>) of pro-B cells. **E)** Average statistics of B220+, CD43+ and IgM+ cells in *Mri*<sup>-/-</sup>*Paxx*<sup>-/-</sup> mice and tested controls. Erythrocytes were lysed during the sample preparation and not counted. Not significant n.s.,  $p > 0,005$ ,  $*p \leq 0,05$ ,  $**p \leq 0,01$ ,  $***p \leq 0,001$ ,  $****p \leq 0,0001$ .



## 5. Discussion

### 5.1 *Xlf<sup>-/-</sup>Paxx<sup>-/-</sup>Trp53<sup>+/-</sup>* deficiency leads to deficient B and T cell development

It is suggested that XLF acts as a bridge between XRCC4 and other recruited factors located at DNA ends [29, 35, 51]. PAXX, on the other hand, is a scaffold to stabilize the Ku heterodimer [10, 35, 51]. Noticeably, single knock out of *Xlf* or *Paxx* genes results in no or modest defects in lymphocyte development in mice [9, 34-37, 44, 53, 54]. However, single inactivation of other NHEJ factors results in blockage of lymphocyte development in mice, e.g. *Dna-pkcs<sup>-/-</sup>* mouse model [35, 41].

Moreover, combined inactivation of *Xlf* and *Paxx* genes results in embryonic lethality in mice [5, 34-36, 44]. Knock out or haploinsufficiency for *Trp53* rescues embryonic lethality of *Xlf<sup>-/-</sup>Paxx<sup>-/-</sup>* mice and allows postnatal survival [5, 35, 46]. *Xlf<sup>-/-</sup>Paxx<sup>-/-</sup>Trp53<sup>+/-</sup>* mice have lower body weight in comparison to the control mice. Besides, there are abnormalities in lymphocyte development of triple deficient mice, such as dramatic reduction of single-positive thymic and splenic T cells (CD4<sup>+</sup> and CD8<sup>+</sup>). Also, the proportion of splenic B cells in *Xlf<sup>-/-</sup>Paxx<sup>-/-</sup>Trp53<sup>+/-</sup>* mice is markedly lower than the examined controls.

Nevertheless, it was unclear whether B lymphocytes mature normally via V(D)J recombination in bone marrow and die before migration to the periphery, or V(D)J recombination are blocked at early stage of B cell development in bone marrow of *Xlf<sup>-/-</sup>Paxx<sup>-/-</sup>Trp53<sup>+/-</sup>* mice. Here, by bone marrow analysis of *Xlf<sup>-/-</sup>Paxx<sup>-/-</sup>Trp53<sup>+/-</sup>* mice, I demonstrated that observed phenotypes are rooted in the bone marrow. Low proportion of B220<sup>+</sup> cells, increased proportion of pro-B cells and reduced proportion of IgM<sup>+</sup> cells in bone marrow of *Xlf<sup>-/-</sup>Paxx<sup>-/-</sup>Trp53<sup>+/-</sup>* mice, suggest that *Xlf<sup>-/-</sup>Paxx<sup>-/-</sup>* double deficiency results in a block in the V(D)J recombination at pro-B cell stage of B cell development in the bone marrow [35]. In conclusion, *Xlf<sup>-/-</sup>Paxx<sup>-/-</sup>Trp53<sup>+/-</sup>* mice possess immunodeficient phenotypes, observed in *Ku70<sup>-/-</sup>*, *Ku80<sup>-/-</sup>*, *Artemis<sup>-/-</sup>* and *Dna-pkcs<sup>-/-</sup>* mouse models [35, 38-41] and reported observations proved my hypothesis.

## 5.2 *Mri*<sup>-/-</sup>*Dna-pkcs*<sup>-/-</sup> double deficiency leads to embryonic lethality

The *Mri*<sup>-/-</sup> mice have normal lymphocyte development [35, 45, 47]. However, the mice lacking NHEJ accessory factor DNA-PKcs, are live-born and possess SCID phenotype [35, 41]. To study the genetic interaction between *Mri* and *Dna-pkcs*, several breeding cages were made as presented in Table 4. According to the mendelian distribution, I should have observed 4 *Mri*<sup>-/-</sup>*Dna-pkcs*<sup>-/-</sup> mice but notably, no *Mri*<sup>-/-</sup>*Dna-pkcs*<sup>-/-</sup> mice were observed.

For further assessment, I examined embryos at embryonic day E14.5, isolated from *Mri*<sup>+/-</sup> *Dna-pkcs*<sup>+/-</sup> female (both parents were *Mri*<sup>+/-</sup> *Dna-pkcs*<sup>+/-</sup>). Two embryos were smaller and lighter when compared to the others. Genotyping PCR confirmed that these two smaller embryos were *Mri*<sup>-/-</sup>*Dna-pkcs*<sup>-/-</sup>. Reported assessments may suggest that *Mri* and *Dna-pkcs*, genes interact genetically and *Mri*<sup>-/-</sup>*Dna-pkcs*<sup>-/-</sup> mice are embryonically lethal. However, more mice need to be genotyped (totally 100-400 mice) in the future.

### 5.3 There is no genetic interaction between *Mri* and *Paxx* genes in mice

*Mri* and PAXX are NHEJ accessory factors. *Mri* is a regulator of NHEJ repair system during S and G2 phases [11, 35, 45]. While, PAXX is a scaffold to stabilize the Ku heterodimer [9, 10, 51]. Noticeably, single deficient *Mri*<sup>-/-</sup> and *Paxx*<sup>-/-</sup> mice have normal lymphocyte development [34-36, 44, 45, 47, 51]. I hypothesized that *Mri* and *Paxx* interact genetically and have overlapping functions in general and lymphocyte development in mice.

Following, various *Mri.Paxx* breeding cages were made (Table 5) to obtain *Mri*<sup>-/-</sup>*Paxx*<sup>-/-</sup> mice. Markedly, mice with combined inactivation of *Mri* and *Paxx* were live-born and showed normal B and T lymphocyte development. The mentioned data in results part highlighting that *Mri*<sup>-/-</sup>*Paxx*<sup>-/-</sup> mice show a similar phenotype as *Mri*<sup>-/-</sup> and *Paxx*<sup>-/-</sup> single knock out controls [35].

Reported observations show that *Mri* and *Paxx* genes are not functionally redundant which disproved my third hypothesis.

## 6. Conclusion

1. *Xlf<sup>-/-</sup>Paxx<sup>-/-</sup>Trp53<sup>+/-</sup>* mice possess deficient B and T cell development. B cell development is arrested at the pro-B stage of development in bone marrow of *Xlf<sup>-/-</sup>Paxx<sup>-/-</sup>Trp53<sup>+/-</sup>* mice.
2. *Mri<sup>-/-</sup>Dna-pkcs<sup>-/-</sup>* mice are embryonically lethal. *Mri* and *Dna-pkcs* genes interact genetically.
3. *Mri* and *Paxx* do not interact genetically. *Mri<sup>-/-</sup>Paxx<sup>-/-</sup>* mice have normal lymphocyte development.

## 7. Future directions

Unhesitatingly, more mice need to be analyzed to determine the genetic interaction between *Mri* and *Dna-pkcs* genes in mice, up to 100 to 400 pups. I hypothesized that the massive apoptosis in the central nervous system (CNS) is the cause of the observed phenotype of tested *Mri/Dna-pkcs* double-deficient embryos, as it was shown earlier for other NHEJ deficient mice such as *Lig4*<sup>-/-</sup> [35, 43], *Xrcc4*<sup>-/-</sup> [35, 42], *Xlf*<sup>-/-</sup>*Mri*<sup>-/-</sup> [35] or *Xlf*<sup>-/-</sup> *Paxx*<sup>-/-</sup> [35, 51] mice.

H&E staining method, using hematoxylin and eosin stains, can be used for brain samples to screen apoptotic bodies and necrotic infarctions in the brain as described earlier for other genotypes [55]. Moreover, the genomic instability using T-FISH assay [6, 9, 48, 50, 54, 56] can be studied in *Mri*<sup>-/-</sup>*Dna-pkcs*<sup>-/-</sup> model as well. I hypothesized that genomic instability is increased in *Mri*<sup>-/-</sup>*Dna-pkcs*<sup>-/-</sup> mice when compared to WT and single knock out controls.

## 8. References

1. Sancar, A., et al., *Molecular mechanisms of mammalian DNA repair and the DNA damage checkpoints*. Annu Rev Biochem, 2004. **73**: p. 39-85.
2. Jung, D., et al., *Mechanism and control of V(D)J recombination at the immunoglobulin heavy chain locus*. Annu Rev Immunol, 2006. **24**: p. 541-70.
3. Kumar, V., F.W. Alt, and V. Oksenysh, *Functional overlaps between XLF and the ATM-dependent DNA double strand break response*. DNA Repair (Amst), 2014. **16**: p. 11-22.
4. Zhang, W.W. and G. Matlashewski, *Single-Strand Annealing Plays a Major Role in Double-Strand DNA Break Repair following CRISPR-Cas9 Cleavage in Leishmania*. mSphere, 2019. **4**(4).
5. Castaneda-Zegarra, S., et al., *Generation of a Mouse Model Lacking the Non-Homologous End-Joining Factor Mri/Cyren*. Biomolecules, 2019. **9**(12).
6. Oksenysh, V., et al., *Functional redundancy between the XLF and DNA-PKcs DNA repair factors in V(D)J recombination and nonhomologous DNA end joining*. Proc Natl Acad Sci U S A, 2013. **110**(6): p. 2234-9.
7. Pannunzio, N.R., G. Watanabe, and M.R. Lieber, *Nonhomologous DNA end-joining for repair of DNA double-strand breaks*. J Biol Chem, 2018. **293**(27): p. 10512-10523.
8. Scully, R., et al., *DNA double-strand break repair-pathway choice in somatic mammalian cells*. Nat Rev Mol Cell Biol, 2019. **20**(11): p. 698-714.
9. Gago-Fuentes, R., et al., *Normal development of mice lacking PAXX, the paralogue of XRCC4 and XLF*. FEBS Open Bio, 2018. **8**(3): p. 426-434.
10. Ochi, T., et al., *DNA repair. PAXX, a paralog of XRCC4 and XLF, interacts with Ku to promote DNA double-strand break repair*. Science, 2015. **347**(6218): p. 185-188.
11. Arnoult, N., et al., *Regulation of DNA repair pathway choice in S and G2 phases by the NHEJ inhibitor CYREN*. Nature, 2017. **549**(7673): p. 548-552.
12. Soubeyrand, S., et al., *Threonines 2638/2647 in DNA-PK are essential for cellular resistance to ionizing radiation*. Cancer Res, 2003. **63**(6): p. 1198-201.
13. Ma, Y., et al., *Hairpin opening and overhang processing by an Artemis/DNA-dependent protein kinase complex in nonhomologous end joining and V(D)J recombination*. Cell, 2002. **108**(6): p. 781-94.
14. Uziel, T., et al., *Requirement of the MRN complex for ATM activation by DNA damage*. Embo j, 2003. **22**(20): p. 5612-21.
15. Turenne, G.A., et al., *Activation of p53 transcriptional activity requires ATM's kinase domain and multiple N-terminal serine residues of p53*. Oncogene, 2001. **20**(37): p. 5100-10.
16. Kindt, T., R. Goldsby, and B. Osborne, *Kuby Immunology 6th ed*, ed. W.H.F.a. Company. 2006.
17. Jenni Punt (author), S.A.S.a., Patricia P Jones (author), Judith A Owen (author), Janis Kuby, Judith A Owen, *Kuby Immunology Eighth edition*. 2018.
18. LeBien, T.W. and T.F. Tedder, *B lymphocytes: how they develop and function*. Blood, 2008. **112**(5): p. 1570-80.
19. Charles A Janeway, J., Paul Travers, Mark Walport, and Mark J Shlomchik., *Immunobiology, 5th edition*. 2001.
20. Bruce Alberts, A.J., Julian Lewis, Martin Raff, Keith Roberts, and Peter Walter., *Molecular Biology of the Cell, 4th edition*. 2002.
21. Bassing, C.H., W. Swat, and F.W. Alt, *The mechanism and regulation of chromosomal V(D)J recombination*. Cell, 2002. **109 Suppl**: p. S45-55.
22. Alt, F.W., et al., *Ordered rearrangement of immunoglobulin heavy chain variable region segments*. Embo j, 1984. **3**(6): p. 1209-19.

23. Caccia, N., et al., *The T cell receptor beta chain genes are located on chromosome 6 in mice and chromosome 7 in humans*. Cell, 1984. **37**(3): p. 1091-9.
24. Lefranc, M.P. and T.H. Rabbitts, *Two tandemly organized human genes encoding the T-cell gamma constant-region sequences show multiple rearrangement in different T-cell types*. Nature, 1985. **316**(6027): p. 464-6.
25. Pan-Hammarstrom, Q., et al., *Reexamining the role of TACI coding variants in common variable immunodeficiency and selective IgA deficiency*. Nat Genet, 2007. **39**(4): p. 429-30.
26. Corneo, B., et al., *Identical mutations in RAG1 or RAG2 genes leading to defective V(D)J recombinase activity can cause either T-B-severe combined immune deficiency or Omenn syndrome*. Blood, 2001. **97**(9): p. 2772-6.
27. Volk, T., et al., *DCLRE1C (ARTEMIS) mutations causing phenotypes ranging from atypical severe combined immunodeficiency to mere antibody deficiency*. Hum Mol Genet, 2015. **24**(25): p. 7361-72.
28. Enders, A., et al., *A severe form of human combined immunodeficiency due to mutations in DNA ligase IV*. J Immunol, 2006. **176**(8): p. 5060-8.
29. Buck, D., et al., *Cernunnos, a novel nonhomologous end-joining factor, is mutated in human immunodeficiency with microcephaly*. Cell, 2006. **124**(2): p. 287-99.
30. Hase, K., et al., *Activation-induced cytidine deaminase deficiency causes organ-specific autoimmune disease*. PLoS One, 2008. **3**(8): p. e3033.
31. Marciano, B.E. and S.M. Holland, *Primary Immunodeficiency Diseases: Current and Emerging Therapeutics*. Front Immunol, 2017. **8**: p. 937.
32. Notarangelo, L.D., *Primary immunodeficiencies*. J Allergy Clin Immunol, 2010. **125**(2 Suppl 2): p. S182-94.
33. Vignesh, P., A. Rawat, and S. Singh, *An Update on the Use of Immunomodulators in Primary Immunodeficiencies*. Clin Rev Allergy Immunol, 2017. **52**(2): p. 287-303.
34. Abramowski, V., et al., *PAXX and Xlf interplay revealed by impaired CNS development and immunodeficiency of double KO mice*. Cell Death Differ, 2018. **25**(2): p. 444-452.
35. Castañeda-Zegarra, S., et al., *Leaky severe combined immunodeficiency in mice lacking non-homologous end joining factors XLF and Mri*. bioRxiv, 2020: p. 2020.03.04.976829.
36. Balmus, G., et al., *Synthetic lethality between PAXX and XLF in mammalian development*. Genes Dev, 2016. **30**(19): p. 2152-2157.
37. Li, G., et al., *Lymphocyte-specific compensation for XLF/cernunnos end-joining functions in V(D)J recombination*. Mol Cell, 2008. **31**(5): p. 631-40.
38. Gu, Y., et al., *Growth retardation and leaky SCID phenotype of Ku70-deficient mice*. Immunity, 1997. **7**(5): p. 653-65.
39. Nussenzweig, A., et al., *Requirement for Ku80 in growth and immunoglobulin V(D)J recombination*. Nature, 1996. **382**(6591): p. 551-5.
40. Rooney, S., et al., *Leaky Scid phenotype associated with defective V(D)J coding end processing in Artemis-deficient mice*. Mol Cell, 2002. **10**(6): p. 1379-90.
41. Gao, Y., et al., *A targeted DNA-PKcs-null mutation reveals DNA-PK-independent functions for KU in V(D)J recombination*. Immunity, 1998. **9**(3): p. 367-76.
42. Gao, Y., et al., *A critical role for DNA end-joining proteins in both lymphogenesis and neurogenesis*. Cell, 1998. **95**(7): p. 891-902.
43. Frank, K.M., et al., *Late embryonic lethality and impaired V(D)J recombination in mice lacking DNA ligase IV*. Nature, 1998. **396**(6707): p. 173-7.
44. Liu, X., et al., *PAXX promotes KU accumulation at DNA breaks and is essential for end-joining in XLF-deficient mice*. Nat Commun, 2017. **8**: p. 13816.
45. Castañeda-Zegarra, S., et al., *Generation of a Mouse Model Lacking the Non-Homologous End-Joining Factor Mri/Cyren*. Biomolecules, 2019. **9**(12).
46. Castaneda-Zegarra, S., et al., *Synthetic lethality between DNA repair factors Xlf and Paxx is rescued by inactivation of Trp53*. DNA Repair (Amst), 2019. **73**: p. 164-169.

47. Hung, P.J., et al., *MRI Is a DNA Damage Response Adaptor during Classical Non-homologous End Joining*. Mol Cell, 2018. **71**(2): p. 332-342.e8.
48. Xing, M., et al., *Synthetic lethality between murine DNA repair factors XLF and DNA-PKcs is rescued by inactivation of Ku70*. DNA Repair (Amst), 2017. **57**: p. 133-138.
49. Mani, R., et al., *Defining genetic interaction*. Proc Natl Acad Sci U S A, 2008. **105**(9): p. 3461-6.
50. Xing, M. and V. Oksenych, *Genetic interaction between DNA repair factors PAXX, XLF, XRCC4 and DNA-PKcs in human cells*. FEBS Open Bio, 2019. **9**(7): p. 1315-1326.
51. Castañeda-Zegarra, S., et al., *Synthetic lethality between DNA repair factors Xlf and Paxx is rescued by inactivation of Trp53*. DNA Repair (Amst), 2019. **73**: p. 164-169.
52. Jacks, T., et al., *Tumor spectrum analysis in p53-mutant mice*. Curr Biol, 1994. **4**(1): p. 1-7.
53. Vera, G., et al., *Cernunnos deficiency reduces thymocyte life span and alters the T cell repertoire in mice and humans*. Mol Cell Biol, 2013. **33**(4): p. 701-11.
54. Dewan, A., et al., *Robust DNA repair in PAXX-deficient mammalian cells*. FEBS Open Bio, 2018. **8**(3): p. 442-448.
55. Mengying, Z., et al., *Apoptosis and necroptosis of mouse hippocampal and parenchymal astrocytes, microglia and neurons caused by Angiostrongylus cantonensis infection*. Parasit Vectors, 2017. **10**(1): p. 611.
56. Oksenych, V., et al., *Functional redundancy between repair factor XLF and damage response mediator 53BP1 in V(D)J recombination and DNA repair*. Proc Natl Acad Sci U S A, 2012. **109**(7): p. 2455-60.



## 9. Supplementary information

### 9.1 Appendix A. Scientific article (co-author) published in 2019.





biomolecules



Article

## Generation of a Mouse Model Lacking the Non-Homologous End-Joining Factor Mri/Cyren

Sergio Castañeda-Zegarra <sup>1,2,†</sup> , Camilla Huse <sup>1,2,†</sup>, Øystein Røsand <sup>1,2,†</sup>, Antonio Sarno <sup>1,2</sup>, Mengtan Xing <sup>1,2</sup>, Raquel Gago-Fuentes <sup>1,2</sup>, Qindong Zhang <sup>1,2</sup>, Amin Alirezaylavasani <sup>1,2</sup>, Julia Werner <sup>1,2,3</sup>, Ping Ji <sup>1</sup>, Nina-Beate Liabakk <sup>1</sup>, Wei Wang <sup>1</sup>, Magnar Bjørås <sup>1,2</sup> and Valentyn Oksenyich <sup>1,2,4,\*</sup> 

<sup>1</sup> Department of Clinical and Molecular Medicine (IKOM), Norwegian University of Science and Technology, 7491 Trondheim, Norway; sergio.m.c.zegarra@ntnu.no (S.C.-Z.); camilhus@stud.ntnu.no (C.H.); oystein.rosand@ntnu.no (Ø.R.); antonio.sarno@ntnu.no (A.S.); mengtan.xing@ntnu.no (M.X.); raquel.gago-fuentes@ntnu.no (R.G.-F.); qindongz@stud.ntnu.no (Q.Z.); aminalir@stud.ntnu.no (A.A.); julia.werner@stud.uni-heidelberg.de (J.W.); ping.ji@ntnu.no (P.J.); nina.beate.liabakk@ntnu.no (N.-B.L.); wei.wang@ntnu.no (W.W.); magnar.bjoras@ntnu.no (M.B.)

<sup>2</sup> St. Olavs Hospital, Trondheim University Hospital, Clinic of Medicine, Postboks 3250, Sluppen, 7006 Trondheim, Norway

<sup>3</sup> Molecular Biotechnology MS programme, Heidelberg University, 69120 Heidelberg, Germany

<sup>4</sup> Department of Biosciences and Nutrition (BioNut), Karolinska Institutet, 14183 Huddinge, Sweden

\* Correspondence: valentyn.oksenych@ntnu.no; Tel.: +47-913-43-084

† These authors contributed equally to this work.

Received: 7 November 2019; Accepted: 26 November 2019; Published: 28 November 2019



**Abstract:** Classical non-homologous end joining (NHEJ) is a molecular pathway that detects, processes, and ligates DNA double-strand breaks (DSBs) throughout the cell cycle. Mutations in several NHEJ genes result in neurological abnormalities and immunodeficiency both in humans and mice. The NHEJ pathway is required for V(D)J recombination in developing B and T lymphocytes, and for class switch recombination in mature B cells. The Ku heterodimer formed by Ku70 and Ku80 recognizes DSBs and facilitates the recruitment of accessory factors (e.g., DNA-PKcs, Artemis, Paxx and Mri/Cyren) and downstream core factor subunits X-ray repair cross-complementing group 4 (XRCC4), XRCC4-like factor (XLF), and DNA ligase 4 (Lig4). Accessory factors might be dispensable for the process, depending on the genetic background and DNA lesion type. To determine the physiological role of Mri in DNA repair and development, we introduced a frame-shift mutation in the Mri gene in mice. We then analyzed the development of Mri-deficient mice as well as wild type and immunodeficient controls. Mice lacking Mri possessed reduced levels of class switch recombination in B lymphocytes and slow proliferation of neuronal progenitors when compared to wild type littermates. Human cell lines lacking Mri were as sensitive to DSBs as the wild type controls. Overall, we concluded that Mri/Cyren is largely dispensable for DNA repair and mouse development.

## 9.2 Appendix B

### PCR Programs

	DNA-PKcs (wt)			DNA-PKcs (mut)			XLF (wt&mut)					
	Time	Degrees	Cycles	Time	Degrees	Cycles	Time	Degrees	Cycles			
Denaturation	3 m	94		3 m	94		3 m	95				
Denaturation	45 s	94	30	45 s	94	40	30 s	95	40			
Annealing	45 s	66		45 s	59.5		1 m	62				
Elongation	1 m	72		1 m	72		5 m	68				
Elongation	5 m	72		5 m	72			4				
		4			4							
MRI (428 bp)			MRI (238 bp)			Trp53 (wt&mut)			PAXX (wt&mut)			
	Time	Degrees	Cycles	Time	Degrees	Cycles	Time	Degrees	Cycles	Time	Degrees	Cycles
Denaturation	5 m	95		5 m	95		2 m	95		2 m	94	-
Denaturation	30 s	95	35	30 s	95	35	30 s	95	30	30 s	94	30
Annealing	30 s	60		30 s	57		30 s	67		45 s	68	
Elongation	40 s	68		40 s	68		20 s	72		1 m	72	
Elongation	5 m	68		5 m	68		5 m	72		5 m	72	-
		4						4		-	4	-

## 9.3 Appendix C

### Primers information

Primer	Sequence	Amplicon
Paxx-1-fw	ACAGAGGGTGGTGACTCAGACAATGG	wt-950 // mut-309, 312, 298
Paxx-2-rev	GGAAATGCTATTAGAACCACTGCCACG	
Dna-pkcs-1-wt	GAAAAAGTCTATGAGCTCCTGGGAG	wt-250 // mut-427
Dna-pkcs-2-common	CCCTCCAGACAGCCAGCTAAGACAGG	
Dna-pkcs-3-mut	ACGTAACCTCCTCTCAGACCT	
Trp53-common	TGGATGGTGGTATACTCAGAGC	wt-321 // mut-150
Trp53-mut	CAGCCTCTGTTCCACATACT	
Trp53-wt	AGGCTTAGAGGTGCAAGCTG	
Xlf-common	GAGCTCGGATATGAGCGCTCAG	wt-650 // mut-950
Xlf-wt	CATGTTGGCTCTGCGAATAGA	
Xlf-mut	CTGTCTTGTGGGCATAGTAGGC	
MRI-F	TCAGGTCTGCCCTACTGA	
MRI-R-428bp-wt	GTGGTGGTGCTTCTCTGTGA	
MRI-R-234-wt	AGAGGGGAGGACCC	

